Proteomic Characterization of the Heart and Skeletal Muscle Reveals Widespread Arginine ADP-Ribosylation by the ARTC1 Ectoenzyme

Leutert, Mario ; Menzel, Stephan ; Braren, Rickmer ; Rissiek, Björn ; Hopp, Ann-Katrin ; Nowak, Kathrin ; Bisceglie, Lavinia ; Gehrig, Peter ; Li, Hui ; Zolkiewska, Anna ; Koch-Nolte, Friedrich ; Hottiger, Michael O

Abstract: The clostridium-like ecto-ADP-ribosyltransferase ARTC1 is expressed in a highly restricted manner in skeletal muscle and heart tissue. Although ARTC1 is well studied, the identification of ARTC1 targets in vivo and subsequent characterization of ARTC1-regulated cellular processes on the proteome level have been challenging and only a few ARTC1-ADP-ribosylated targets are known. Applying our recently developed mass spectrometry-based workflow to C2C12 myotubes and to skeletal muscle and heart tissues from wild-type mice, we identify hundreds of ARTC1-ADP-ribosylated proteins whose modifications are absent in the ADP-ribosylome of ARTC1-deficient mice. These proteins are ADP-ribosylated on arginine residues and mainly located on the cell surface or in the extracellular space. They are associated with signal transduction, transmembrane transport, and muscle function. Validation of hemopexin (HPX) as a ARTC1-target protein confirmed the functional importance of ARTC1-mediated extracellular arginine ADP-ribosylation at the systems level.

DOI: https://doi.org/10.1016/j.celrep.2018.07.048

Resource

Cell Reports

Proteomic Characterization of the Heart and Skeletal Muscle Reveals Widespread Arginine ADP-Ribosylation by the ARTC1 Ectoenzyme

Graphical Abstract

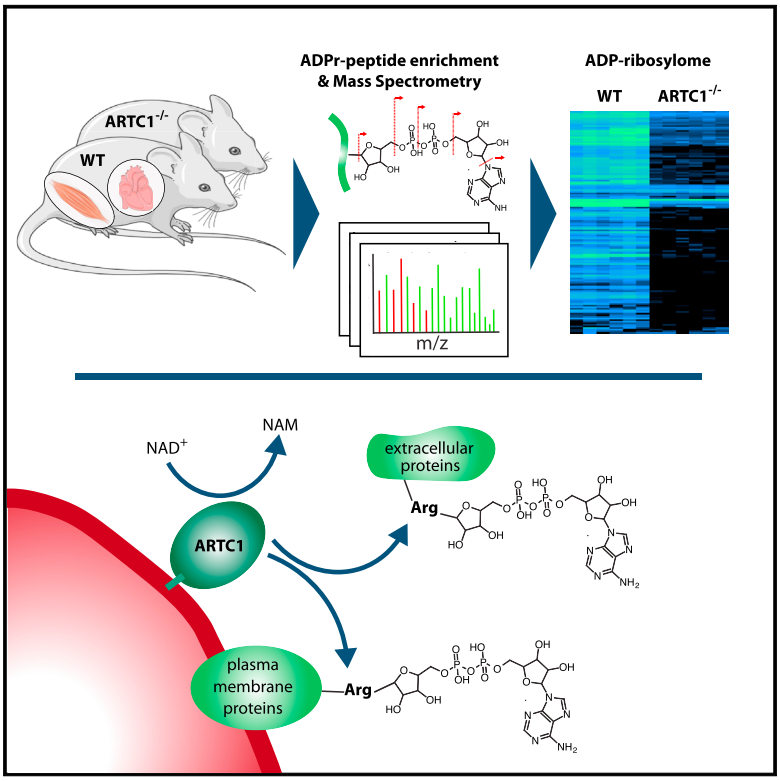

Highlights

- Ectoenzyme ARTC1 ADP-ribosylates hundreds of proteins in muscle and heart tissue
- ARTC1 ADP-ribosylates arginine residues on extracellular domains of target proteins
- ARTC1-deficient mice show signs of muscle weakness
- ADP-ribosylation of hemopexin by ARTC1 modulates its heme binding activity *in vitro*

Authors

Mario Leutert, Stephan Menzel, Rickmer Braren, ..., Anna Zolkiewska, Friedrich Koch-Nolte, Michael O. Hottiger

Correspondence

nolte@uke.de (F.K.-N.), michael.hottiger@dmmd.uzh.ch (M.O.H.)

In Brief

Leutert et al. identify the ADP-ribosylomes of skeletal muscle and heart tissue and show that they comprise mainly arginine modification sites that are modified by the ADP-ribosyltransferase ARTC1. The functional importance of ARTC1 is documented by impaired muscle performance in ARTC1-deficient mice and tuning of heme binding by hemopexin ADP-ribosylation *in vitro*.

Leutert et al., 2018, Cell Reports *24*, 1916–1929
August 14, 2018
https://doi.org/10.1016/j.celrep.2018.07.048

CellPress

OPEN ACCESS
CellPress

Cell Reports
Resource

Proteomic Characterization of the Heart and Skeletal Muscle Reveals Widespread Arginine ADP-Ribosylation by the ARTC1 Ectoenzyme

Mario Leutert,[1,2,6] Stephan Menzel,[3] Rickmer Braren,[3,7] Björn Rissiek,[3,8] Ann-Katrin Hopp,[1,2] Kathrin Nowak,[1,2] Lavinia Bisceglie,[1,2] Peter Gehrig,[4] Hui Li,[5,9] Anna Zolkiewska,[5] Friedrich Koch-Nolte,[3,10,*] and Michael O. Hottiger[1,10,11,*]

[1]Department of Molecular Mechanisms of Disease, University of Zurich, Winterthurerstrasse 190, 8057 Zurich, Switzerland
[2]Molecular Life Science PhD Program of the Life Science Zurich Graduate School, Winterthurerstrasse 190, 8057 Zurich, Switzerland
[3]Institute of Immunology, University Medical Center Hamburg-Eppendorf, Martinistrasse 52, 20246 Hamburg, Germany
[4]Functional Genomics Center Zurich, University of Zurich, Winterthurerstrasse 190, 8057 Zurich, Switzerland
[5]Department of Biochemistry and Molecular Biophysics, Kansas State University, 141 Chalmers Hall, Manhattan, KS 66506, USA
[6]Present address: Department of Genome Sciences, University of Washington, Seattle, WA 98195, USA
[7]Present address: Institute of Diagnostic and Interventional Radiology, Klinikum Rechts der Isar der Technischen Universität München, Munich, Germany
[8]Present address: Department of Neurology, University Medical Center Hamburg-Eppendorf, Hamburg, Germany
[9]Present address: Department of Molecular Biology, University of Texas Southwestern Medical Center, Dallas, TX, USA
[10]Senior author
[11]Lead Contact
*Correspondence: nolte@uke.de (F.K.-N.), michael.hottiger@dmmd.uzh.ch (M.O.H.)
https://doi.org/10.1016/j.celrep.2018.07.048

SUMMARY

The clostridium-like ecto-ADP-ribosyltransferase ARTC1 is expressed in a highly restricted manner in skeletal muscle and heart tissue. Although ARTC1 is well studied, the identification of ARTC1 targets *in vivo* and subsequent characterization of ARTC1-regulated cellular processes on the proteome level have been challenging and only a few ARTC1-ADP-ribosylated targets are known. Applying our recently developed mass spectrometry-based workflow to C2C12 myotubes and to skeletal muscle and heart tissues from wild-type mice, we identify hundreds of ARTC1-ADP-ribosylated proteins whose modifications are absent in the ADP-ribosylome of ARTC1-deficient mice. These proteins are ADP-ribosylated on arginine residues and mainly located on the cell surface or in the extracellular space. They are associated with signal transduction, transmembrane transport, and muscle function. Validation of hemopexin (HPX) as a ARTC1-target protein confirmed the functional importance of ARTC1-mediated extracellular arginine ADP-ribosylation at the systems level.

INTRODUCTION

Protein ADP-ribosylation is an ancient post-translational modification (PTM) found in a wide range of biological species (Corda and Di Girolamo, 2003; Koch and Rüger, 1994; Ueda and Hayaishi, 1985). ADP-ribosylation has been shown to regulate several cellular processes by altering the function of the modified protein and/or providing a scaffold for the recruitment of other proteins. ADP-ribosylation can be divided into two subtypes: mono-ADP-ribosylation (MARylation), in which only mono-ADP-ribose (MAR) is transferred to an amino acid of a target protein, and poly-ADP-ribosylation (PARylation), which involves the addition of further ADP-ribose (ADPr) moieties to generate poly-ADP-ribose (PAR) (Hottiger, 2015). In mammalians, these modifications are catalyzed by ADP-ribosyltransferases (ARTs), which are divided into two ART families, ARTC (C2/C3 toxin-like, also ecto-ARTs) and ARTD (diphtheria toxin-like, formerly PARPs), respectively (Hottiger et al., 2010). While all known enzymes catalyzing PARylation belong to the ARTD family, and MARylation has traditionally been the domain of the ARTCs, it has recently been appreciated that some ARTDs and even some structurally unrelated sirtuins can also mediate MARylation (Feijs et al., 2013).

Four human (ARTC1, 3, 4, 5, formerly also hART1-5) and six mouse (ARTC1, 2.1, 2.2, 3, 4, 5, formerly also mART1-5) ARTC genes have been identified. For both species, ARTC1 is expressed mainly in skeletal and heart muscles, non-lactated mammary gland, brown adipocytes, epithelial cells, or activated granulocytes (Braren et al., 1998; Glowacki et al., 2002; Koch-Nolte et al., 2006). The ARTC family members ARTC1–ARTC4 are expressed as glycosylphosphatidylinositol (GPI)-anchored ecto-enzymes (Glowacki et al., 2001, 2002; Hottiger et al., 2010; Koch-Nolte et al., 2006). ARTC1, 2, and 5 contain the characteristic cholera toxin R-S-E catalytic motif in their active center. R and S are important for NAD^+ binding and E has a catalytic function (Laing et al., 2011). Arginine-specific MARylation activity has been confirmed for human and mouse ARTC1 and ARTC5 as well as the two mouse proteins of ARTC2.1 and ARTC2.2 (Glowacki et al., 2002).

An important question when examining the biological function of ARTCs is the endogenous source of extracellular NAD^+ under

normal and pathophysiological conditions, since NAD^+ is not cell membrane permeable and the extracellular and plasma levels of NAD^+ are lower than intracellular NAD^+ concentrations (Davies et al., 1999; Haag et al., 2007; Koch-Nolte et al., 2011). However, NAD^+ can be released from intracellular sources during lytic processes, hypoxia, and inflammation (Adriouch et al., 2007; Bruzzone et al., 2001; Haag et al., 2007; Scheuplein et al., 2009; Seman et al., 2004). The net biological effect of extracellular NAD^+ therefore depends on the amount of NAD^+ released into the extracellular space, the quality and quantity of specific receptors/enzymes expressed, and on the activities of the catabolizing-enzymes (Haag et al., 2007; Koch-Nolte and Ziegler, 2013).

Functional consequences of eukaryotic arginine ADP-ribosylation have mainly been studied for ARTC2.2 targets such as the ion channel P2X7. MARylation of R125 of P2X7 leads to its activation (Adriouch et al., 2008) and subsequent inflammasome activation, processing, and cytokine release (IL-1β, IL-18, IL-1 receptor antagonist and IL-36α), as well as release and activation of proteases (mainly ADAM10 and 17) resulting in the shedding of cell surface molecules, including ARTC2.2 itself (Bartlett et al., 2014; Menzel et al., 2015). Prolonged activation of P2X7 stimulates T cell death, also called NAD^+-induced cell death (NICD) (Adriouch et al., 2007). As for ARTC1, which was found in bronchoalveolar lavage fluid from smokers, it was reported to modify the defensin human neutrophil peptide 1 (HNP1) on Arg14 and Arg24, which specifically reduces its antimicrobial and cytotoxic activities (Paone et al., 2002; Stevens et al., 2009). ARTC1 ADP-ribosylation was also found to have a role in endoplasmic reticulum (ER) stress responses (Fabrizio et al., 2015). In addition, ARTC1 ADP-ribosylates members of the integrin family of adhesion molecules on skeletal muscle cells and leukocytes (Zolkiewska and Moss, 1993). ADP-ribosylation of integrin α7 (ITGA7) by ARTC1 modulates the binding of integrin α7β1 to laminin (Okazaki and Moss, 1999).

Despite these recent discoveries, the substrates of the different ARTCs as well as their implications in cellular processes are still not very well understood. Furthermore, it is also not known whether ARTC1-mediated ADP-ribosylation has any role under steady-state (i.e., basal) conditions. This is in large part due to the fact that mass spectrometry (MS)-based methods were only developed for and applied to the identification of cell culture-derived ADP-ribosylated proteins and their ADPr acceptor sites. Very recently, we developed an approach that allowed the analysis of ADP-ribosylated proteins in the liver, a tissue that has already been described to regulate cellular processes in an ADP-ribosylation-dependent manner (Martello et al., 2016). Interestingly, ARTC2.2 was found among the modified targets. Moreover, we have shown that the GPI-anchored ARTC2.2 is restricted to a small subset of target proteins by its association with lipid rafts but promiscuously modifies many different targets upon detergent solubilization of the plasma membrane (Bannas et al., 2005; Laing et al., 2011). It remained so far unclear whether ARTC1 has a comparable target spectrum, or whether it would only modify a few specific target proteins, as it has been observed for the bacterial ART toxins.

Here, we analyzed the ARTC1-specific ADP-ribosylome in C2C12 myotubes as well as skeletal and heart muscle of wild-type and ARTC1-deficient mice, which were generated to facilitate systems-level analyses. These studies revealed that ARTC1 is essential for the modification of numerous proteins under basal conditions, which provides strong evidence for the physiological importance of ARTC1. In particular, we show that ARTC1-dependent ADP-ribosylation of hemopexin (HPX) strongly reduces its capacity to bind heme, which is likely highly relevant for the function of this strongest known heme binding protein. We provide a comprehensive systems-level analysis of an ARTC1-substrate relationship *in vivo* and map ARTC1-mediated ADP-ribosylation in two different muscle tissues. The site-specific profile of the ARTC1-dependent ADP-ribosylome provides evidence for a widespread contribution of ADP-ribosylation on the cell surface and the extracellular space and provides an extensive resource that allows to further discover the functional relevance of ADP-ribosylation in muscle physiology and pathophysiology.

RESULTS

ARTC1 Mediates Widespread Extracellular ADP-Ribosylation in C2C12 Myotubes

To assess the extent of ARTC1-mediated ADP-ribosylation and to identify ADP-ribosylated proteins, we first verified the expression of ARTC1 in differentiating C2C12 cells by qRT-PCR and could confirm previous reports (Zolkiewska and Moss, 1993) showing that ARTC1 is specifically expressed in mouse heart tissue and C2C12 myotubes (Figure S1A). The other known active membrane-bound extracellular ART expressed in mice is ARTC2 (Koch-Nolte et al., 2008). We were, however, unable to detect ARTC2 in C2C12 myotubes by qRT-PCR (data not shown), which is in agreement with the reports that ARTC2 is predominantly expressed in immune cells (Glowacki et al., 2002; Koch-Nolte et al., 1999). ARTC3 is also present in C2C12 myotubes as detected by a recent proteomics approach (Deshmukh et al., 2015). ARTC3, however, lacks the catalytic R-S-E motif and was therefore proposed to be catalytically inactive (Glowacki et al., 2002). To determine whether ARTC3 is indeed inactive, we employed DC27.10 cells, which were engineered to stably overexpress ARTC1 or ARTC3 (Koch-Nolte et al., 2005). We confirmed overexpression and localization of ARTC1 and ARTC3 to the plasma membrane by flow cytometric analysis (Figure S1B). Incubation of these cells with [^{32}P]-NAD^+ led to strong ADP-ribosylation of cell surface proteins in the case of ARTC1-overexpressing cells, but not in the case of ARTC3-overexpressing or parental cells (Figure S1C). Next, we performed small interfering RNA (siRNA)-mediated knockdown of endogenous ARTC1 and ARTC3 in C2C12 myoblasts and subsequently differentiated them to myotubes (Figure S1D). Addition of [^{32}P]-NAD^+ to those myotubes revealed that cell surface ADP-ribosylation in C2C12 myotubes is exclusively dependent on ARTC1 (Figure S1E).

To assess the target space of ARTC1, we treated differentiated C2C12 myotubes with NAD^+ or left them untreated and subsequently mapped site-specific ADP-ribosylation using our established ADP-ribosylome proteomic workflow (Bilan et al., 2017b; Martello et al., 2016). This method identifies the ADP-ribosylated peptide sequence and the exact ADPr amino acid

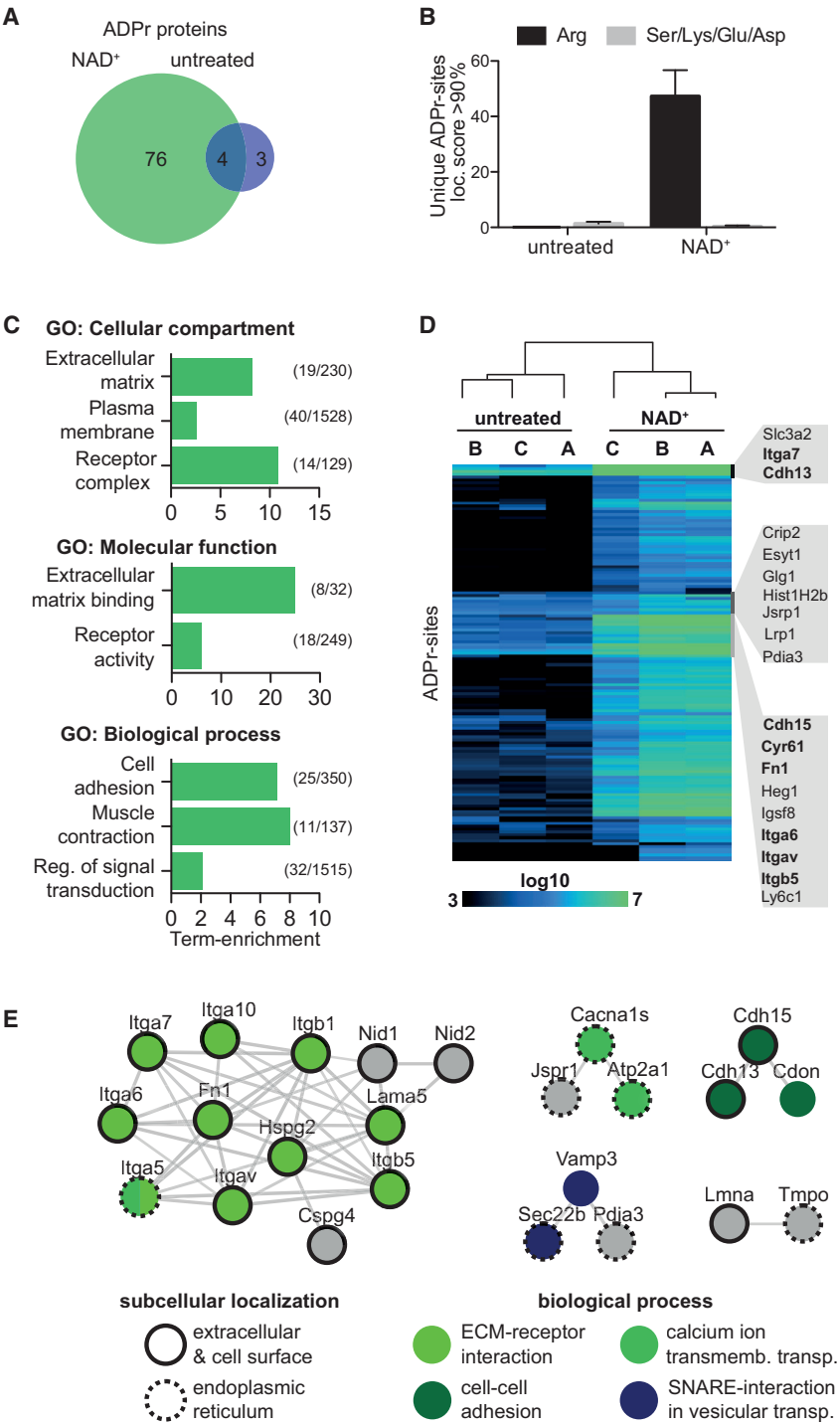

Figure 1. Profiling of ADP-Ribosylation in Mouse Myotubes

(A) Venn diagram of identified unique ADP-ribosylated proteins in C2C12 myotubes left untreated or treated with 50 μM NAD^+.

(B) R-ADP-ribosylation is specifically induced upon NAD^+ treatment of C2C12 myotubes. Identified unique ADPr acceptor sites in C2C12 myotubes left untreated or treated with 50 μM NAD^+ (n = 3; bar graph represents mean and SD).

(C) GO term-enrichment analysis displaying significantly enriched ($p < 0.001$) GO terms of the identified ADP-ribosylated proteins (n = 85) according to their cellular localization, molecular function, and the biological processes. Term enrichment is calculated relative to a deep C2C12 myotube proteome (n = 8,476) (Deshmukh et al., 2015). Numbers in parentheses indicate participation size and category size, respectively.

(D) Unsupervised hierarchical clustering analysis of normalized intensity values determined by MS1-based label-free quantification of detected ADP-ribosylation sites. A black cell corresponds to an absent or a relatively low-abundant ADP-ribosylation site, blue indicates a site of intermediate abundance, and green indicates a highly abundant site. Protein names for three indicated clusters, where ADPr peptides are observed already under untreated conditions are indicated. Names in bold correspond to proteins with a function in biological adhesion.

(E) STRING database analysis of high-confidence protein interactions (interaction score, >0.7) between identified ADP-ribosylated proteins in C2C12 cells. Only ADP-ribosylated proteins with at least one interaction with another ADP-ribosylated protein are shown. Subcellular localization and biological process are annotated.

See also Figures S1 and S2 and Table S1.

acceptor site with a high probability (mascot site localization score, >90%) for ~22% of the identified modified peptides in this study. While only few modified peptides were identified under basal (i.e., untreated) conditions, we identified a strong increase in ADP-ribosylation following NAD^+ treatment (144 versus 9 unique ADP-ribosylated peptides [Figure S2A]; 80 versus 7 ADP-ribosylated proteins [Figure 1A] corresponding to 120 ± 47 versus 9 ± 1 ADP-ribosylated peptide spectra matches [Figure S2B]). Under these conditions, arginine was identified as the main ADPr-acceptor amino acid (Figure 1B). Gene ontology (GO) analyses revealed that the NAD^+ treatment-dependent ADP-ribosylation targets are predominantly extracellular and plasma membrane proteins having a molecular function in extracellular matrix binding and receptor activity and participating in biological processes associated with cell adhesion, muscle contraction, and regulation of signal transduction (Figure 1C).

To quantitatively assess the observed increase of ADP-ribosylation, we performed label-free MS1-based quantification of all identified ADP-ribosylated peptides using three biological replicates of untreated and NAD^+-treated C2C12 myotubes. A good Pearson correlation of the ADP-ribosylated peptide abundance among untreated ($R > 0.76$) and NAD^+-treated ($R > 0.87$) replicates, respectively, demonstrated that the measured

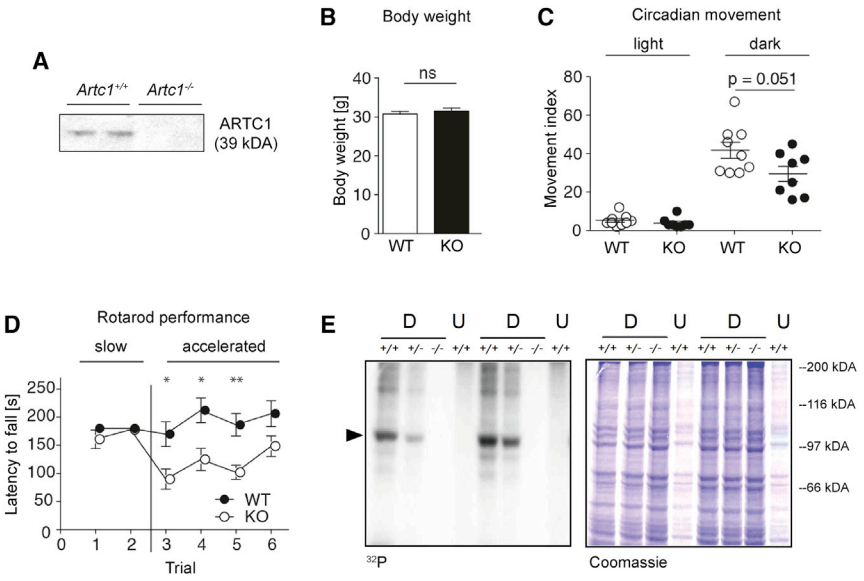

Figure 2. Characterization of the *Artc1*$^{-/-}$ Mouse

(A) Western blotting of glycoprotein-enriched muscle extracts using an anti-ARTC1 antibody confirmed the absence of the 39-kDa ARTC1 protein in *Art1c*$^{-/-}$ mice. Two different mice of WT and *Artc1*$^{-/-}$ genotype were analyzed.

(B) Adult male *Artc1*$^{-/-}$ mice (n = 8) have similar average weights as their WT littermates (n = 9; bar graph represents mean and SD).

(C) Monitoring of voluntary activity using the Mouse E-Motion system. Mice were placed in individual cages, and movements were recorded in three consecutive 12-hr light/12-hr dark cycles. Data points represent the activity of individual mice over 72 hr, expressed as the movement index ± SEM (Student's t test).

(D) Endurance of muscle activity was assessed using the rotarod performance system. Mice were adapted to the rotarod at low speed (4 rpm) in trials 1 and 2. Trials 3–5 were then performed at an accelerated speed (8 rpm) with a pause of 45 min between each trial. Trial 6 was performed the next day at the accelerated speed. The maximum duration of mice staying on the rotarod was 5 min. The latency to fall for each group is expressed as mean ± SEM (Student's t test, *p < 0.05; **p < 0.01).

(E) Primary myoblasts isolated from six littermate pups (genotypes shown at the top), differentiated (D) *in vitro* into myotubes or undifferentiated (U), were incubated with [^{32}P]-NAD$^+$ and analyzed by SDS-PAGE and autoradiography (left panel) or Coomassie blue staining (right panel). Position of a prominent ADP-ribosylated protein is indicated on the left, and molecular weight markers (kDa) are on the right.

See also Figure S3.

ADP-ribosylated peptide signal intensities could be used as a reliable measure for modification site abundance (Figure S2C). Most detected ADP-ribosylated targets were strongly induced upon NAD$^+$ treatment and, importantly, are novel ARTC1 targets (Figure 1D; Table S1). The heatmap representation of the ADP-ribosylation site abundance reveals three minor clusters of sites that were already stably ADP-ribosylated under basal conditions (Figure 1D). From the indicated clusters, the ADP-ribosylated peptides of the top and lower cluster were more abundantly modified after NAD$^+$ treatment and included four members of the integrin family (ITGA7, ITGA6, ITGAV, and ITGB5) (Figure 1D), with ITGA7 representing the only previously reported ARTC1 target (Zolkiewska and Moss, 1993). A small portion of the ADP-ribosylation sites identified remained largely unchanged following NAD$^+$ treatment as visualized in the middle cluster. This cluster included histone H2B, which however is unlikely a target of ARTC1, since the two proteins are not in the same cellular compartment (Leidecker et al., 2016; Martello et al., 2016). Interestingly, most of the proteins of this small middle cluster (approximately 80%) were annotated to be localized to the endomembrane system, and thus likely not affected by addition of exogenous NAD$^+$.

To understand whether several members of protein complexes are targeted by ADP-ribosylation, we mapped and visualized high-confidence interactions (minimum required interaction scores, >0.7) between the ADP-ribosylated proteins identified above using the STRING database of physical and functional protein interactions (Szklarczyk et al., 2015). The analysis identified several protein interaction networks that were abundantly ADP-ribosylated but revealed no significant enrichment of ADP-ribosylation targeting multiple members of protein complexes. We could unravel an interaction network of 13 ADP-ribosylated proteins with a high enrichment in extracellular matrix (ECM)-receptor interactions, suggesting that ADP-ribosylation of this ECM interaction complex might specifically modulate its function in cell adhesion and ECM-receptor signaling (Figure 1E). The other interacting protein groups that were identified function in cell-cell adhesion, calcium ion transmembrane transport, and vesicular transport (Figure 1E). In summary, these data show that differentiated muscle cells exhibit ARTC1-dependent NAD$^+$-inducible ADP-ribosylation responses that mainly affect plasma membrane and/or extracellular proteins.

ARTC1 Knockout Animals Are Viable and Develop Normally, but Show Reduced Skeletal Muscle ADP-Ribosylation and Signs of Muscle Weakness

To elucidate the role of ARTC1 ADP-ribosylation *in vivo*, we generated ARTC1-deficient (*Artc1*$^{-/-}$) mice. This was achieved via insertion of loxP sites into the *Artc1* gene (Figures S3A–S3D). Transgene-positive offspring were mated with a deleter strain, which resulted in the generation of *Artc1*$^{-/-}$ knockout animals. *Artc1* gene deletion was confirmed by PCR and ARTC1 protein absence in muscle tissue by western blotting of a glycoprotein-enriched muscle extract (Figures S3E and 2A). *Artc1*$^{-/-}$ mice were fertile and did not show any overt phenotype. The overall body constitution as judged by body weight did not seem to be overtly impaired (Figure 2B). We did observe a slight reduction in circadian movement, which could be due to muscle weakness (Figure 2C). Consistently, *Artc1*$^{-/-}$ mice showed signs of muscle weakness in an accelerated rotarod test (Figure 2D), suggesting that the lack of ARTC1 affects the skeletal or heart muscle function. Next, we wanted to confirm the importance of

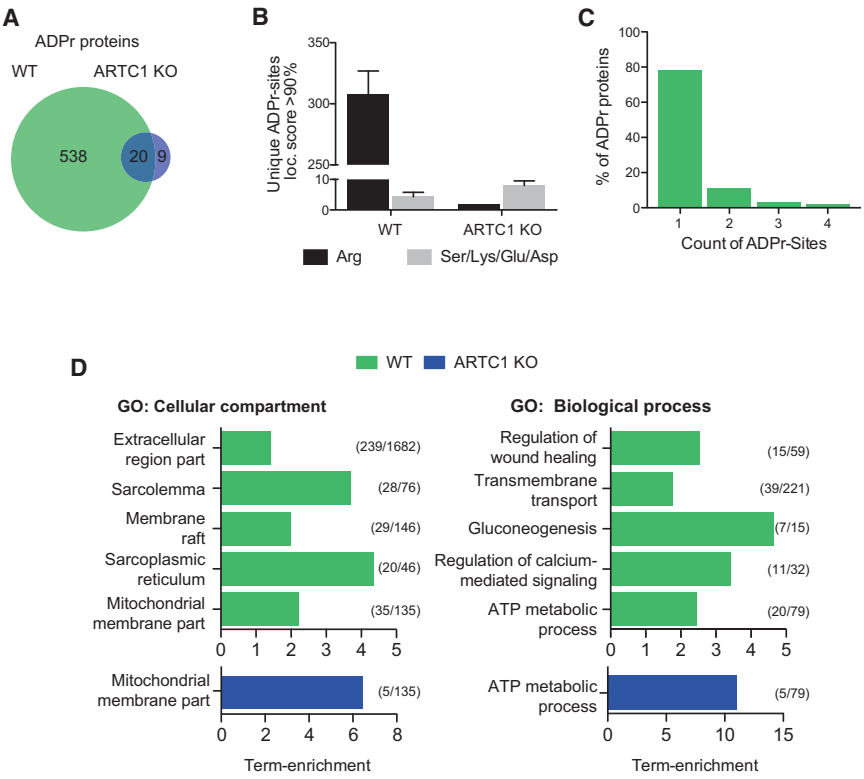

Figure 3. Profiling of ADP-Ribosylation in Skeletal Muscle

(A) The ADP-ribosylome of skeletal muscle is strongly dependent on ARTC1. Venn diagram of unique identified ADP-ribosylated proteins in skeletal muscle tissue from WT and *Artc1*$^{-/-}$ mice (three animals per group).

(B) R-ADP-ribosylation in skeletal muscle tissue is strongly ARTC1 dependent. Identified ADPr acceptor sites in WT and *Artc1*$^{-/-}$ skeletal muscle tissue (n = 3; bar graph represents mean and SD).

(C) Histogram analysis shows that the majority (78%) of ADP-ribosylated skeletal muscle proteins carry only one ADPr modification.

(D) Term-enrichment analysis displaying significantly enriched ($p < 0.001$) GO terms of the identified ADP-ribosylated proteins in WT (n = 573) and *Artc1*$^{-/-}$ (n = 33) tissue according to their cellular localization and the biological processes. Term enrichment is calculated relative to a deep mouse skeletal muscle proteome (n = 5,647) (Deshmukh et al., 2015). Numbers in parentheses indicate participation size and category size, respectively. See also Figure S3 and Table S2.

ARTC1 for muscle cell ADP-ribosylation. To this end, primary myoblasts from wild-type (WT) and *Artc1*$^{-/-}$ mice were differentiated *in vitro* and treated with radioactively labeled NAD^+. Autoradiograms showed complete absence of surface protein ADP-ribosylation in *Artc1*$^{-/-}$ myotubes, while WT and heterozygous cells displayed an *Artc1* gene dose-dependent ADP-ribosylation signal (Figure 2E). Furthermore, the dominant band at ~100 kDa, is undetectable in the *Artc1*$^{-/-}$ samples (Figure 2E). A similar radiolabeled band was previously observed in C2C12 myotubes and was identified as the heavy chain of integrin alpha 7, based on differential mobility in SDS-PAGE under reducing/non-reducing conditions, binding to a laminin affinity column, co-immunoprecipitation with anti-integrin beta 1 antibody, and amino acid sequencing (Zolkiewska and Moss, 1993, 1995). Together, these results confirm that ARTC1 is essential in differentiated muscle cells for ADP-ribosylation of cell surface proteins and hint at a functional *in vivo* relevance for ARTC1-mediated ADP-ribosylation in skeletal and heart muscle.

ARTC1 Is Essential for the Skeletal Muscle ADP-Ribosylation *In Vivo*

Having established the *Artc1*$^{-/-}$ mice, we aimed to define the *in vivo* ARTC1-dependent ADP-ribosylome of murine skeletal muscle. Total skeletal muscle protein extracts from unstressed WT and *Artc1*$^{-/-}$ mice were prepared in a denaturing guanidine-HCl lysis buffer, and the ADP-ribosylated fraction was enriched and subsequently analyzed by MS as described earlier (Martello et al., 2016). Importantly, these animals were perfused with the ARTC inhibitor Novobiocin prior to muscle extraction to inhibit extraction-induced ADP-ribosylation. MS analyses identified a large basal ADP-ribosylome in WT animals that consisted of 1,318 unique ADP-ribosylated peptides (Figure S3F; Table S2), corresponding to 558 ADP-ribosylated proteins (Figure 3A). Good correlations were observed between biological replicates (Figure S3G). Moreover, a >20-fold reduction in the number of unique ADPr-peptides in *Artc1*$^{-/-}$ muscle tissues was observed, strongly indicating that ARTC1 is the main writer of skeletal muscle ADP-ribosylation under basal conditions (Figure S3F). The importance of ARTC1 for the muscle ADP-ribosylome was further validated by ADPr-acceptor site specificity analyses. As expected for ARTC1 targets (Koch-Nolte, 2015), the vast majority of the ADPr-acceptor sites identified in WT tissues were Arg residues, which were almost completely absent in the corresponding *Artc1*$^{-/-}$ samples (Figure 3B). In fact, the remaining ADP-ribosylated proteins observed in *Artc1*$^{-/-}$ muscles were modified on Ser, Lys, Glu, or Asp residues. Over 70% of the ADP-ribosylated proteins in WT muscle tissues carried only a single modification (Figure 3C), which suggests that ARTC1-dependent ADP-ribosylation is a tightly controlled and targeted process. These findings were further substantiated by GO analyses, which demonstrated that the identified ADP-ribosylated proteins localized to extracellular, membrane, and/or mitochondrial compartments and function in transmembrane transport, calcium signaling, and/or ATP metabolic processes (Figure 3D). ADP-ribosylated proteins from *Artc1*$^{-/-}$ muscle only showed a significant enrichment in mitochondrial proteins having a role in ATP-metabolic processes.

Together, these experiments provide evidence that ARTC1 modifies a defined set of proteins already under unstressed conditions and that the observed skeletal muscle ADP-ribosylome is rather stable. When comparing the ADP-ribosylomes of WT

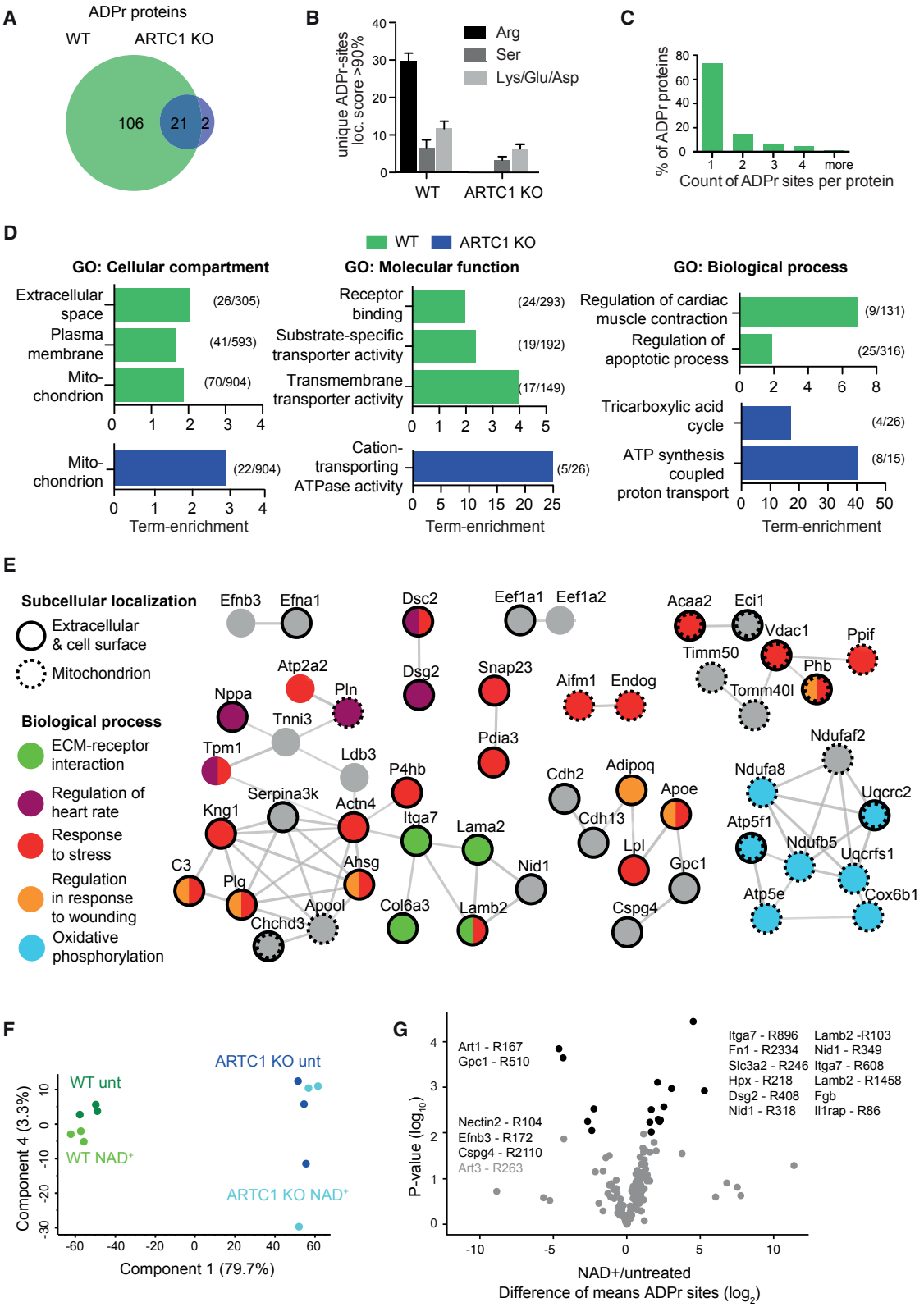

Figure 4. Profiling of the Mouse Heart ADP-Ribosylome

(A) The ADP-ribosylome of the heart tissue is strongly dependent on ARTC1. Venn diagram of unique identified ADP-ribosylated proteins in heart muscle tissue from WT and *Artc1*$^{-/-}$ mice (three animals per group).

(legend continued on next page)

skeletal muscle and C2C12 myotubes, we found that around 37% of the ADP-ribosylated proteins identified in NAD^+-treated C2C12 myotubes were also modified in the skeletal muscle (Figure S3H).

The ARTC1-Dependent Heart and Skeletal Muscle ADP-Ribosylomes Differ

To investigate whether ARTC1 activity or the obtained skeletal muscle ADP-ribosylome is specific to this tissue or shares similarities with heart tissue, ADP-ribosylome analyses were performed on mouse hearts from WT and *Artc1*$^{-/-}$ mice. Compared to the skeletal muscle, less ADP-ribosylation sites were identified in WT hearts under basal conditions; however, Arg was still the most abundant ADP-ribosylation site and was strongly reduced in the corresponding *Artc1*$^{-/-}$ tissues (Figures 4A, 4B, and S4A; Table S3). Around 85% of the observed ADP-ribosylation sites were dependent on ARTC1 (Figure S4A). The performed MS analyses were reproducible with 70% and 60% of the ADP-ribosylated proteins identified in at least two biological replicates for the WT and the *Artc1*$^{-/-}$ tissue samples, respectively (Figure S4B). The variation in the measurement of non-ARTC1-mediated targets was substantially larger than of ARTC1 targets. Closer analyses of the ADP-ribosylation sites revealed preferential modification of Arg residues in WT heart tissues only, while Ser, Lys, Glu, or Asp residues were the only sites identified in *Artc1*$^{-/-}$ hearts (Figure 4B). Similar to what was observed in skeletal muscle (Figure 3C), approximately 70% of the modified proteins that were identified in mouse hearts were ADP-ribosylated at only one site (Figure 4C).

To characterize the mouse heart ADP-ribosylome in more detail, the ADP-ribosylome data were subjected to GO analysis, which produced a pattern of term enrichment similar to what was observed for skeletal muscle. WT heart samples were enriched for proteins that localize to the plasma membrane and/or extracellular space, function in receptor binding and/or transporter activity, and are involved in the regulation of muscle contraction and apoptotic processes. In contrast, these terms were absent from the ADP-ribosylomes identified in the *Artc1*$^{-/-}$ samples, which only showed enrichment for mitochondrial proteins and proteins involved in the trichloroacetic acid (TCA) cycle and ATP synthesis (Figure 4D). This suggests that ARTC1 most probably manifests its functionality by ADP-ribosylation of a broad array of membrane-associated and extracellular protein targets. To analyze whether specific protein complexes would be ADP-ribosylated and whether the modified proteins functionally co-regulate certain cellular processes, STRING-based protein-protein interaction analyses were carried out for ADP-ribosylated proteins identified either exclusively in WT (Figure 4E) or *Artc1*$^{-/-}$ animals (i.e., ARTC1-independent targets; Figure S4C). Nine high-confidence interaction networks of ADP-ribosylated proteins were identified exclusively in the WT heart muscle samples (Figure 4E). These interaction networks mostly contained extracellular and plasma membrane proteins that are involved in stress responses. Similar to the C2C12 cells, we found an interaction network of ADP-ribosylated proteins that mediates ECM-receptor interactions but also identified heart-specific functional interaction networks. Interestingly, we identified an ADP-ribosylated protein network that plays a role in oxidative phosphorylation and is situated in the mitochondria; however, these proteins were not modified at Arg and therefore unlikely ARTC1 targets. In fact, this network fits better to the pattern observed in the *Artc1*$^{-/-}$ animals. There we identified three ARTC1-independent ADP-ribosylated protein networks for mostly mitochondrial and some cytosolic proteins that function in oxidative phosphorylation, TCA cycle, and fatty acid degradation (Figure S4C).

Although we started our analyses with the same amount of protein (i.e., from heart and skeletal muscle) and observed quite a large overlap (60%) of ADP-ribosylated proteins identified in the heart compared to the skeletal muscle tissues (compare Figure 3A to Figure 4A and Figure S4D), four times more ADP-ribosylated proteins were identified in skeletal compared to heart muscle tissues. To test our sample-handling regime that was focused on eliminating ADP-ribosylation reactions due to tissue extraction and sample preparation, we tested lysis of the tissue under different conditions (Figure S4E). The lysis was performed either with a modified RIPA buffer (Larsen et al., 2017) or a denaturing 6 M guanidine-HCl buffer (Poulsen et al., 2013) in combination with Novobiocin perfusion, as already performed previously with the skeletal muscle samples. In addition, animals were pretreated with Novobiocin (intravenous [i.v.], 30 min before sacrifice). MS analysis of these three samples revealed that guanidine-HCl lysis buffer prevented lysis-induced ADP-ribosylation since pretreatment with Novobiocin i.v. did not reduce the observed amount of modification. On the other hand, modified RIPA buffer alone was not able to prevent lysis-induced ADP-ribosylation, which resulted in an increased number of identified ADP-ribosylated peptides (compared to

(B) R-ADP-ribosylation in heart tissue is strongly ARTC1 dependent. Identified ADPr acceptor sites in WT and *Artc1*$^{-/-}$ heart tissue (n = 3; bar graph represents mean and SD).

(C) Histogram analysis shows that the majority (71%) of ADP-ribosylated heart proteins carry only one ADPr modification.

(D) GO term-enrichment analysis displaying significantly enriched ($p < 0.001$) GO terms of the identified ADP-ribosylated proteins in WT (n = 131) and *Artc1*$^{-/-}$ (n = 26) tissues according to their cellular localization, molecular function, and the biological processes. Term enrichment is calculated relative to a deep mouse heart proteome (n = 3,157) (Lau et al., 2016). Numbers in parentheses indicate participation size and category size, respectively.

(E) STRING database analysis of high-confidence interaction (interaction score, >0.7) between identified ADP-ribosylated proteins in heart tissue, dependent on ARTC1 expression. Only ADP-ribosylated proteins with at least one interaction with another ADP-ribosylated protein are shown. Subcellular localization and biological process are annotated.

(F) Principal-component analysis of the abundance of ADP-ribosylated peptides from WT and *Artc1*$^{-/-}$ hearts that were NAD^+ treated or left untreated (three animals per group).

(G) Volcano plot analysis of WT heart untreated versus NAD^+ treated. Significantly different sites are shown in black (FDR < 0.5) and ADP-ribosylation sites are annotated.

See also Figures S4–S6 and S10 and Table S3.

guanidine-HCl) consistent with our previous findings for ARTC2.2 (Bannas et al., 2005) (Figure S4E).

The reduced ADP-ribosylation in the heart could also be due to different plasma membrane compositions (i.e., affecting ARTC1 complex formation) in heart and muscle, which might affect ARTC1 activity and affinity to NAD^+, or due to overall less NAD^+ in the heart tissue. To test whether the lower amount of ADP-ribosylation is due to lack of substrate in healthy unstressed mouse hearts, animals were pretreated with NAD^+ (i.v.) 30 min before sacrifice, the hearts were harvested, and ADP-ribosylome MS analysis was performed. Injection of NAD^+ did not increase the overall number of identified ADP-ribosylated peptides significantly, neither in WT nor in *Artc1*$^{-/-}$ background (Figure S5A). Moreover, NAD^+ pretreatment altered neither the ADPr acceptor site profile nor the number of unique ADPr acceptor sites significantly (Figure S5B). To strengthen this aspect, we aimed at detecting potential quantitative changes of ADP-ribosylation after NAD^+ treatment by applying a label-free MS1 quantification approach. Replicate comparison of the signal intensities of ADP-ribosylated peptides revealed a very strong Pearson correlation among the triplicates of untreated and NAD^+-treated WT tissues (>0.92) and a lower but acceptable correlation among the *Artc1*$^{-/-}$ replicates (>0.73), respectively (Figure S5C). Principal-component analyses of ADP-ribosylated peptide abundance revealed that the ADP-ribosylomes of untreated and NAD^+-pre-treated WT hearts differed and segregated in two groups, whereas the *Artc1*$^{-/-}$ heart samples were much more variable and NAD^+ treatment did not seem to induce distinct changes, indicating that when ARTC1 was absent, the NAD^+ treatment did not have an effect on ADP-ribosylation (Figure 4F). Quantitative MS analysis of three independent samples confirmed that NAD^+ treatment of WT mice induces only little *de novo* protein ADP-ribosylation but leads to quantitative changes of discrete ADP-ribosylation sites, most of them already present in untreated hearts (Figures 4G and S5D). Interestingly, after applying statistical cutoffs, this analysis showed that 12 ADP-ribosylation sites were significantly more abundant after the NAD^+ treatment, including sites on integrin alpha 7 and HPX, and that five ADP-ribosylation sites were less abundant after the treatment, including ADP-ribosylation on ARTC1 itself (Figure 4G). The NAD^+ treatment only changed the degree of the ADP-ribosylation at specific sites of these proteins; however, total protein level remained constant for the ones we could quantify by label-free quantification (LFQ) of the total proteome before enrichment (Figure S6A). Integrin alpha 7, which has been shown before *in vitro* to be a target of ARTC1, shows the most significantly induced ADP-ribosylation (on Arg896 and Arg608) after NAD^+ treatment, which is in line with our results from NAD^+-treated myotubes. Also, integrin alpha 7 interacting ECM proteins LAMB2 showed a significant increase of ADP-ribosylation at two sites (Arg103 and Arg1458). Moreover, a significantly increased proportion of ADP-ribosylation on the two soluble extracellular proteins HPX and Fibronectin1 (FN1) could be detected upon NAD^+ treatment (Figure 4G). In contrast, ARTC1 itself, ARTC3, GPC1, NECTIN2, CSPG4, and EFNB3, all of them plasma membrane proteins, were less abundantly modified after NAD^+ treatment. The reduction in modification on these proteins could be due to shedding by metalloproteases, which would sequester them from the membrane-bound ARTC1 (Buchanan et al., 2017; Janes et al., 2009; Kawahara et al., 2017; Menzel et al., 2015; Sakry et al., 2014).

Apart from ARTC1, we also found ARTC3 to be ADP-ribosylated in WT skeletal and heart muscle tissue, but not in *Artc1*$^{-/-}$ tissue. This indicates that ARTC3 is ADP-ribosylated by ARTC1, especially since no significant changes in total ARTC3 protein levels could be observed in the different WT and *Artc1*$^{-/-}$ tissue samples (Figure S6B).

Arginine ADP-Ribosylation Motifs and Marker Ion

We attempted to identify an Arg-ADP-ribosylation consensus motif as previously identified for nuclear Ser-ADP-ribosylation (Bilan et al., 2017a; Bonfiglio et al., 2017). Analysis of a 21-aa window with the identified Arg-ADP-ribosylation sites in the middle revealed five significantly enriched motifs ($p < 0.0005$, binomial test), comprising 78%, 30%, and 63% of all identified Arg-ADP-ribosylation sites in C2C12, skeletal muscle, and heart muscle, respectively (Figure 5). The most prominent motif identified consisted in an R(-ADPr)G motif (in all sample types), followed by an RR(-ADPr) motif (in skeletal and heart muscle).

We noticed that a large portion of ADP-ribosylated peptides contain missed cleavage sites. In the case of our skeletal muscle dataset, we found that ~70% contained one missed cleavage site, whereas ~60% of non-modified peptides showed no missed cleavage (Figure S7A). Most missed cleavage sites include ADP-ribosylated arginine residues, with the likely explanation of sterical hindrance of trypsin binding. In contrast to unmodified peptides, we identified a large proportion of missed cleavage site with arginines at the first position of ADP-ribosylated peptides, ~25% in skeletal muscle (Figure S7B). These arginines were almost exclusively identified as ADP-ribosylation sites and mainly belonged to the RR(-ADPr) motif identified above. This suggests that trypsin is able to recognize and cleave after an arginine or lysine preceding a modified arginine residue; however, it is not able to process the modified residue itself. This has been observed for serine ADP-ribosylation as well (Bonfiglio et al., 2017). To further validate the presence of modified arginines at the first position of the peptides, we performed a small-scale Lys-C protease (cleaves only after lysine) and trypsin digest on the same skeletal muscle sample. Interestingly, in contrast to the tryptic digest, Lys-C digestion resulted for both, non-modified and ADP-ribosylated peptides, in less than 5% missed cleavage sites (Figure S7C), indicating that arginine ADP-ribosylation blocks trypsin recognition of the modified amino acid but exhibits less hindrance of protease processing of adjacent or close-by sites. ADP-ribosylated peptides derived from Lys-C digestion suffered generally from lower ADP-ribosylation site localization probabilities compared to tryptic ADP-ribosylated peptides (Figure S7D). The data generated by the Lys-C experiment was not extensive enough to predict statistically relevant ADP-ribosylation motifs. However, we were still able to validate identified RR(ADPr) sites in Lys-C-derived peptides (Figure S8A) and could prove that these sites can indeed exist as tryptic peptides with a missed cleaved and modified arginine in the first position (Figure S8B) or as Lys-C peptides with an internal ADP-ribosylation site (Figures S8C and S9).

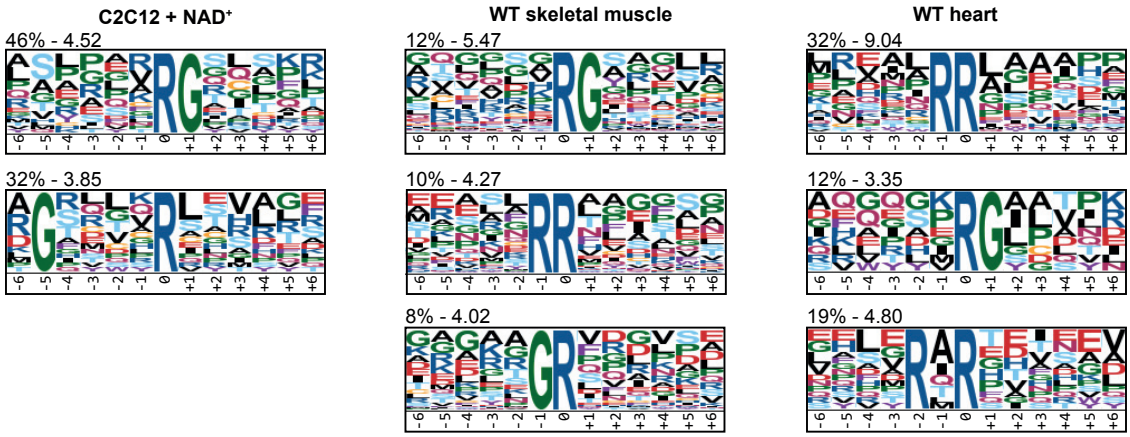

Figure 5. Arginine ADP-Ribosylation Motifs

R/G and R/R motifs identified at Arg-ADP-ribosylation sites with a localization probability of >90% in C2C12 cells, WT muscle, and heart tissue compared against the whole mouse proteome as background (binomial test, $p < 0.0005$) using x-motif (Chou and Schwartz, 2011). Percentage of all Arg-ADP-ribosylation sites containing the motif and motif score are shown on top of the respective sequence motif.

See also Figures S7–S10.

Studies of *in vitro*-modified peptides have suggested that ADP-ribosylated Arg residues can give rise to an Arg-specific ADPr marker ion (ADPr-carbodiimide; Figure S10A) during MS2 fragmentation (Osago et al., 2009).

Due to the unusual elemental composition of ADPr-carbodiimide, which contains two phosphate groups, its accurate *m/z* value (584.09019) can easily be distinguished from any peptide fragment ion by using Orbitrap mass analyzers. ADPr marker ions can be extracted from MS2 spectra and have proven beneficial in the identification and validation of ADP-ribosylated peptides (Bilan et al., 2017a). We screened MS2 spectra from the measured heart samples using the PTM marker finder R-package to extract ADPr marker ions (Nanni et al., 2013; Panse and Grossmann, 2012). When we screened for spectra containing at least four ADPr marker ions, we could identify 361 spectra containing an ADPr-carbodiimide ion (10% of spectra) in the WT samples and only 3 in *Artc1*$^{-/-}$ samples (0.9% of spectra) (Figure S10B). As expected, ADPr-carbodiimide ions showed a lower intensity than the other marker ions; however, in many cases they were readily identified and could be used to estimate the Arg-specific ADP-ribosylation levels (Figures S10B and S10C).

ADP-Ribosylation of HPX Reduces Its Capacity to Bind Heme

To validate our findings, we investigated the functional relevance of HPX ADP-ribosylation, which was identified on Arg-218 in heart and skeletal muscle tissue. HPX is the strongest known heme binder (Tolosano and Altruda, 2002) and plays a crucial role during inflammatory conditions by scavenging heme (Tolosano and Altruda, 2002). To confirm that HPX is a direct ARTC1 target, recombinant HPX was incubated with ARTC1 and radiolabeled NAD^+. We found that recombinant ARTC1 modified HPX *in vitro* and that no glycation or passive attachment of NAD^+ to HPX occurs (Figure 6A). ARTC1-dependent HPX modification was sensitive to ARTC inhibitor Novobiocin and slightly decreased in the presence of heme (Figure 6B). MS analysis of the *in vitro* reaction confirmed the ADP-ribosylation of Arg218 *in vitro* and additionally identified ADP-ribosylation on R83. Manual annotation of higher-energy collision dissociation (HCD) and electron-transfer/higher-energy collision dissociation (EThcD) fragmentation spectra for *in vivo*- and *in vitro*-modified HPX peptides confirmed ADP-ribosylation on Arg218 and revealed Arg-ADP-ribosylation-specific ADPr-carbodiimide ions and losses of the corresponding neutral fragments (Figure 6C). Arg218 faces the heme binding pocket of HPX and might therefore interfere with heme binding upon ADP-ribosylation (Figure 6D). To test this possibility, a heme binding assay measuring the HPX-heme protein complex formation absorbance at 413 nm was established (Hvidberg et al., 2005). ADP-ribosylated HPX was strongly impaired in its heme binding capacity as compared to unmodified HPX (Figures 6E and 6F), indeed suggesting that the ADP-ribosylation of HPX might regulate its heme binding capacity and might therefore be a physiologically relevant function.

DISCUSSION

In this study, we investigated the targets of ARTC1 in C2C12 myotubes, as well as in skeletal and heart muscle tissues at the systems level. These proteome-profiling studies, which compared tissues from WT and *Artc1*$^{-/-}$ mice, uncovered a large, previously unidentified ARTC1-dependent ADP-ribosylome composed of mainly membrane and secreted proteins that were most often modified on a single Arg. Ser, Lys, Glu, and Asp modifications were also identified, but these ADP-ribosylation events were not dependent on ARTC1. We showed that Arg-specific ADP-ribosylation could be additionally confirmed using a diagnostic ADPr-carbodiimide ion specific for the modified Arg for ~10% of the Arg-ADPr-peptide spectra. Comparison of the identified peptides revealed sequence motifs with enriched Gly and Arg adjacent to the modified Arg within ARTC1 target proteins.

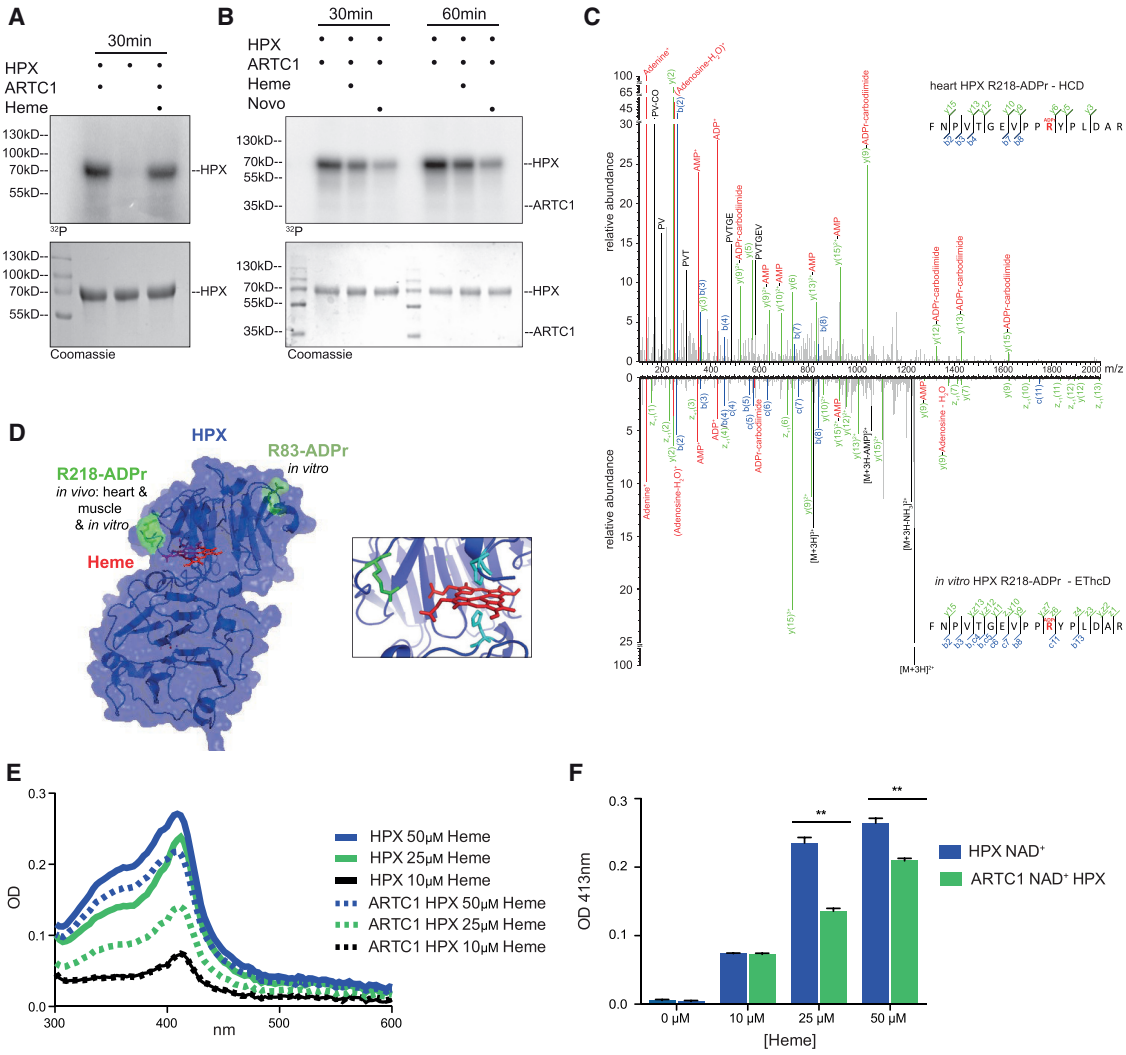

Figure 6. ARTC1-Mediated ADP-Ribosylation of HPX Interferes with Heme Binding

(A) Autoradiography of mouse hemopexin (HPX) *in vitro* ADP-ribosylation by recombinant mouse ARTC1 or NAD^+ alone. Heme (10 μM) was added to indicated reactions.

(B) Autoradiography of mouse HPX *in vitro* ADP-ribosylation by recombinant mouse ARTC1. Heme (10 μM) or Novobiocin (10 μM) were added to indicated reactions.

(C) Manual annotation of high-resolution HCD (top) and EThcD (bottom) MS2 fragmentation spectrum of a HPX peptide confirms ADP-ribosylation on R218. Spectra were retrieved from measured WT heart tissue and *in vitro* modified HPX, respectively. The y and z ion series are shown in green, the b and c ion series are in blue, and the ADPr-specific marker ions and neutral losses are indicated in red.

(D) Crystal structure of HPX bound to heme (red) (Paoli et al., 1999) with indicated ADP-ribosylation sites. The ADPr sites on Arg218 detected in WT heart and skeletal muscle might interfere with HPX ability to sequester heme due to its very close proximity to the heme-binding site. ADP-ribosylated Arg218 and Arg83 are highlighted.

(E) Absorbance measurement of non-modified HPX (HPX incubated with NAD^+) or ADP-ribosylated HPX (HPX incubated with NAD^+ and ARTC1) incubated in the presence of different concentrations of heme. Average absorbance measurement from 300 to 600 nm for the different reactions in triplicates are shown; the HPX-heme complex absorbs light at 413 nm.

(F) ARTC1-mediated ADP-ribosylation of HPX inhibits heme binding *in vitro*. Binding was assessed as in (E) and OD413 is shown as a bar plot for triplicate measurement of the indicated reactions (n = 3; bar graph represents mean and SD, t test, $^{**}p < 0.01$).

Based on the vast amount of proteins identified under untreated conditions *in vivo*, ARTC1 seems to be constitutively active and to play a role under steady-state conditions, which is in stark contrast to the intracellular stress-responsive ARTD1–3. The very strong drop in the number of detectable ADP-ribosylation sites in *Artc1*$^{-/-}$ compared to WT mice strongly suggests that ARTC1 is the main contributor to the skeletal and heart ADP-ribosylome under untreated conditions (Figures 2 and 3). ARTC2.2 was not expressed in C2C12 or the tested tissues. ARTC3 is expressed in C2C12 cells; however, it

did not show any detectable catalytic activity. Furthermore, expression of ARTC3 is independent of ARTC1 expression and it does not contribute to the ADP-ribosylome. Nevertheless, ARTC3 was detected as an ADP-ribosylated protein in WT skeletal and heart muscle tissue, but not in the *Artc1*$^{-/-}$ tissue. On the basis of these findings, we propose that ARTC3 is modified by ARTC1, even though we cannot rule out the possibility that ARTC3 shows weak automodification activity.

NAD^+ can be released upon necrosis or mechanical stress in tissue, which could activate ARTCs during organ collecting (Koch-Nolte et al., 2011). Considering that ARTCs have higher affinity for NAD^+ compared to intracellular ARTDs, ARTCs are more prone to activation following NAD^+ release during tissue collecting (Koch-Nolte et al., 2011). The ADP-ribosylomes we profiled were quite stable and constrained to the extracellular compartment, the plasma membrane, the ER, and the mitochondria with modification of many low-abundant proteins. STRING analysis identified modification of multiple interacting proteins involved in ECM-receptor interaction, cell adhesion, and transmembrane transport, suggesting that ARTC1 might unfold its biological potential by targeting whole protein complexes.

Much of the identified intracellular Arg-ADP-ribosylation is detected in the endomembrane system (as identified by GO term-enrichment analysis) and likely corresponds to protein modification occurring during maturation (ER and Golgi) as both ARTC1 and its target proteins are processed in and traffic through these compartments. The mitochondrial proteins might be ADP-ribosylated non-enzymatically due to the high NAD^+ concentration in the mitochondria (Koch-Nolte et al., 2011) or by an unknown mitochondrial ART. Alternatively, the finding of some cytoplasmic and mitochondrial Arg-ADP-ribosylated proteins could mean that the applied extraction procedure might in some cases still lead to ADP-ribosylation of intracellular proteins due to tissue damage induced upon excising the tissues, as previously reported for ARTC2.2 (Bannas et al., 2005). It will be interesting to test whether ARTC1-mediated ADP-ribosylation also has a function in endogenously occurring tissue damage.

The remarkable stability of the observed ARTC1-mediated ADP-ribosylomes contrasts with the induced ADP-ribosylomes catalyzed by ARTD1 upon oxidative stress, which can be detected only for a few minutes (Martello et al., 2016). Reversibility of cell surface ADP-ribosylation was previously studied on integrin alpha 7 revealing that surface ADP-ribosylation is not readily reversed by ADP-ribosylhydrolases (Zolkiewska and Moss, 1995). These findings suggested that the responsible erasers operate outside the postulated ADP-ribosylation cycle. ARH1, the only known arginine-specific ADP-ribosylhydrolase, is solely expressed within the cell, but not secreted. It is thus tempting to speculate that the extracellular ADP-ribosylation could only be removed from the cell membrane proteins by internalization and protein degradation or shedding, potentially rendering the removal of Arg-ADP-ribosylation a slow process. Alternatively, ADPr could also be processed by extracellular phosphodiesterases, thereby converting it to phospho-ribosylated proteins.

Comparison of ADP-ribosylated proteins in the three sample types revealed a 40% overlap between the C2C12 sample and the *in vivo* samples and a 44% overlap between the two *in vivo* muscle sample types. Although the proteome of C2C12 is different from skeletal muscle (44% of the proteins show a different expression profile [Deshmukh et al., 2015]), this does not explain the limited overlap of the ADP-ribosylomes but rather suggests that ARTC1's expression levels, activity, and specificity are different in cell culture compared to *in vivo*. These differences could stem from variations in the ECM and local fluids that control ARTC1 activity. In analogy to ARTC2, it is possible that the targets of ARTC1 are also restricted to raft-associated target proteins (Bannas et al., 2005). Alternatively, differential concentrations of available NAD^+ could lead to a different ADP-ribosylome.

Computational analysis of all modified peptide sequences revealed motifs for many Arg-ADP-ribosylation sites and showed that often another Arg or a Gly residue is positioned adjacent to a modified Arg (Figure 5). The Arg/Arg motif might provide a beneficial environment for the catalytic ART process or might serve as a positively charged protein-protein interaction patch whose functionality could be annihilated by ADP-ribosylation of one of the arginines. A Arg/Arg motif was already observed for individual proteins in *in vitro* ARTC2.2 assays (Adriouch et al., 2008). Interestingly, the Ser modified by ARTD was also found to be adjacent to a positively charged Lys or Arg residue (Bilan et al., 2017a), suggesting that a positively charged amino acid beside the ADPr acceptor site might be important for the biochemical reaction independent whether the modification is catalyzed by ARTC or ARTD family members. The Gly/Arg and Arg/Gly motifs might render the Arg more accessible to ARTC1.

The identification of the Arg-specific ADPr-carbodiimide marker ion for a subset of Arg-ADP-ribosylated peptides in complex samples opens the possibility to include the marker ion in product-dependent MS methods upon optimizing fragmentation energies (Bilan et al., 2017a; Leidecker et al., 2016; Osago et al., 2009; Rosenthal and Hottiger, 2014). This will be beneficial while studying ARTC targets in complex backgrounds by specifically targeting Arg-ADP-ribosylated peptides and thereby acquiring high-quality spectra.

In *ARTC1*$^{-/-}$ samples, also a residual ARTC1-independent ADP-ribosylome could be detected, which was not affected by NAD^+ pretreatment. Our data reveal that these proteins were mainly modified at Ser, Lys, Glu, or Asp. However, these sites were by far less abundant than the identified ARTC1 targets. Compared to the arginine-modified sites, it was difficult to obtain good localization for these alternative modification sites, probably due to their labile ADPr-peptide bond upon MS2 fragmentation (Bonfiglio et al., 2017). These proteins with ARTC1–independent ADP-ribosylation were identified by term enrichment analysis to be involved in metabolic processes and oxidative-reduction processes, and mainly localized to the mitochondria, suggesting that these processes may be influenced by the modification. As mentioned above, the high NAD^+ concentration found in mitochondria might also favor non-enzymatic ADP-ribosylation for these proteins (Koch-Nolte et al., 2011). NAD^+ *i.v.* injection (i.e., a DAMP signal) did not markedly alter the total number of ADP-ribosylated sites of the analyzed heart tissues, but changed their quantitative composition. It is likely that NAD^+ treatment induces a metalloprotease (e.g, ADAM17)

(Menzel et al., 2015), which would lead to shedding of plasma membrane proteins. Indeed, GPC1 as well as NECTIN4, the close relative of NECTIN2, are known to be shed by ADAM17 (Buchanan et al., 2017; Kawahara et al., 2017). CSPG4 and EFNB3 can be cleaved by ADAM10, the close relative of ADAM17 (Buchanan et al., 2017; Janes et al., 2009; Sakry et al., 2014) The soluble form of these proteins might be less efficiently targeted by membrane-bound ARTC1. ARTC2.2, the close relative of ARTC1 and 3, has been shown to be released by ADAM17 (Menzel et al., 2015). Interestingly, the region close to the GPI-anchor where ARTC2.2 is cleaved is conserved in GPI-anchored ARTC1 as well as in ARTC3, indicating that they might also be shed (Menzel et al., 2015). Release of ARTC1 itself might lead to a shift in its activity toward soluble proteins such as HPX and FN1 as shown previously for ARTC2.2 (Menzel et al., 2015). So far, it is not clear which targets are modified by soluble ARTC2.2.

Moreover, we characterized and functionally validated the ADP-ribosylation of HPX using purified recombinant proteins and observed that *in vitro* modification of HPX strongly interfered with its capacity to bind heme (Figure 6). HPX is a soluble protein that it is usually found in heart and skeletal muscle tissue (Deshmukh et al., 2015; Lau et al., 2016). After acute hemolysis (e.g., after post-ischemic reperfusion or sepsis), excess heme is bound by HPX (Fasano et al., 2005). HPX-heme complexes are taken up by macrophages or hepatocytes and heme is degraded (Hvidberg et al., 2005). HPX is also important for heme export from cells, by accepting heme from export proteins, indicating that HPX also has a function directly at the plasma membrane, placing it in the potential vicinity of ARTC1 (Yang et al., 2010). The inhibitory role of ARTC1-mediated ADP-ribosylation might thus play a role in heme homeostasis by shifting the binding of heme to other proteins and reduce heme degradation under non-stressed conditions. Interestingly, a recent report provides evidence that post-translational oxidative modification of HPX's Tyr199, which is in close structural proximity to R218, also impairs heme binding (Hahl et al., 2017).

The identified ARTC1 target proteins seem to be involved in various pathways controlling muscle function, which might explain the observed reduced endurance of the muscle activity in *Artc1*$^{-/-}$ mice. Whether this observation is only due to skeletal, heart, or both muscle tissues needs to be further addressed. ARTC1 is GPI-anchored and seems to be concentrated in lipid rafts at the cell surface. This topology could regulate ARTC1's specificity to other membrane proteins associated with lipid rafts (Seman et al., 2004). The STRING analyses surprisingly identified a modified protein network in the mitochondria in WT tissue, which was not detected in *Artc1*$^{-/-}$ tissue. We found that these mitochondrial ADP-ribosylation sites are lower abundant than the extracellular ARTC1 targets, making them more prone to biological as well as sample and measurement variations.

Together, we identified and compared the ADP-ribosylomes of the murine skeletal muscle and heart tissue, and we showed that they are largely ARTC1 dependent. Furthermore, our system-level analyses show that, *in vivo*, ARTC1 has an immense target space, which is remarkably stable. We provide a rich resource for ARTC-mediated ADP-ribosylation research, which was so far limited to a few targets and cumbersome biochemical identification of sites by site-directed mutations and *in vitro* experiments. The ADPr-acceptor site localization database that we provide here contains HCD and EThcD ADPr spectra resource of primary tissue (data are available via ProteomeXchange with identifier PXD008041) and can be used by researchers as a resource to further investigate the functional implication of ADP-ribosylation in muscle tissues.

STAR★METHODS

Detailed methods are provided in the online version of this paper and include the following:

- KEY RESOURCES TABLE
- CONTACT FOR REAGENT AND RESOURCE SHARING
- EXPERIMENTAL MODEL AND SUBJECT DETAILS
  - Generation and Characterization of Artc1$^{-/-}$ Mice
  - Performance Assessment
  - Mouse Treatment and Organ Harvesting for Proteomic Experiment
  - Cell Culture and Treatments
- METHOD DETAILS
  - Gene Expression
  - Flow Cytometry
  - Immunoblotting
  - ADP-Ribosylation Reaction on Cells
  - ADP-Ribosylation Reaction with Recombinant Proteins
  - ADPr-Peptide Enrichment
  - Liquid Chromatography and Mass Spectrometry Analysis
- QUANTIFICATION AND STATISTICAL ANALYSIS
  - Raw Mass Spectrometry Data Analysis and Label Free Quantification
  - Bioinformatic Analyses
- DATA AND SOFTWARE AVAILABILITY
  - Data Availability

SUPPLEMENTAL INFORMATION

Supplemental Information includes ten figures and three tables can be found with this article online at https://doi.org/10.1016/j.celrep.2018.07.048.

ACKNOWLEDGMENTS

We would like to thank Tobias Suter and Deena Leslie Pedrioli (University of Zurich) for the helpful discussions and for providing editorial assistance. We also thank Paolo Nanni, Christian Panse, and Jonas Grossmann from the Functional Genomics Center of the University of Zurich for helpful discussions and advice. We thank the Flow Cytometry Core Facility of the UZH for their support. We thank Marion Nissen and Fabienne Seyfried, Hamburg, for excellent technical assistance. F.K.-N. thank Drs. Nigel Killeen and Dan Littman for their support with ES cell transfections and blastocyst injections and their generous hospitality during their stay as visiting scientists in their lab at the University of California, San Francisco. This work was supported by Grants No310/6 and SFB877/A5 from the DFG to F.K.-N.; M.L. was supported by the Forschungskredit of the University of Zurich; ADP-ribosylation research in the laboratory of M.O.H. is funded by the Kanton of Zurich and the Swiss National Science Foundation (Grants 310030_157019 and 31003A_176177).

AUTHOR CONTRIBUTIONS

M.L., S.M., F.K.-N., and M.O.H. conceived the project and performed data analysis. M.L. and S.M. performed sample preparation, bioinformatics analysis, and, together with P.G., mass spectrometry analysis. R.B., B.R., H.L., and A.Z. generated and analyzed *Artc1*$^{-/-}$ mice. A.-K.H., K.N., and L.B. performed various assays during revisions. M.L. and M.O.H. prepared the manuscript. M.O.H. and F.K.-N. directed and supervised all aspects of the study. All authors critically reviewed the manuscript.

DECLARATION OF INTERESTS

The authors declare no competing interests.

Received: December 22, 2017
Revised: April 19, 2018
Accepted: July 12, 2018
Published: August 14, 2018

REFERENCES

Adriouch, S., Hubert, S., Pechberty, S., Koch-Nolte, F., Haag, F., and Seman, M. (2007). NAD+ released during inflammation participates in T cell homeostasis by inducing ART2-mediated death of naive T cells in vivo. J. Immunol. *179*, 186–194.

Adriouch, S., Bannas, P., Schwarz, N., Fliegert, R., Guse, A.H., Seman, M., Haag, F., and Koch-Nolte, F. (2008). ADP-ribosylation at R125 gates the P2X7 ion channel by presenting a covalent ligand to its nucleotide binding site. FASEB J. *22*, 861–869.

Bannas, P., Adriouch, S., Kahl, S., Braasch, F., Haag, F., and Koch-Nolte, F. (2005). Activity and specificity of toxin-related mouse T cell ecto-ADP-ribosyltransferase ART2.2 depends on its association with lipid rafts. Blood *105*, 3663–3670.

Bartlett, R., Stokes, L., and Sluyter, R. (2014). The P2X7 receptor channel: recent developments and the use of P2X7 antagonists in models of disease. Pharmacol. Rev. *66*, 638–675.

Bilan, V., Leutert, M., Nanni, P., Panse, C., and Hottiger, M.O. (2017a). Combining higher-energy collision dissociation and electron-transfer/higher-energy collision dissociation fragmentation in a product-dependent manner confidently assigns proteomewide ADP-ribose acceptor sites. Anal. Chem. *89*, 1523–1530.

Bilan, V., Selevsek, N., Kistemaker, H.A.V., Abplanalp, J., Feurer, R., Filippov, D.V., and Hottiger, M.O. (2017b). New quantitative mass spectrometry approaches reveal different ADP-ribosylation phases dependent on the levels of oxidative stress. Mol. Cell. Proteomics *16*, 949–958.

Bonfiglio, J.J., Fontana, P., Zhang, Q., Colby, T., Gibbs-Seymour, I., Atanassov, I., Bartlett, E., Zaja, R., Ahel, I., and Matic, I. (2017). Serine ADP-ribosylation depends on HPF1. Mol. Cell *65*, 932–940.e6.

Braren, R., Glowacki, G., Nissen, M., Haag, F., and Koch-Nolte, F. (1998). Molecular characterization and expression of the gene for mouse NAD+:arginine ecto-mono(ADP-ribosyl)transferase, Art1. Biochem. J. *336*, 561–568.

Bruzzone, S., Guida, L., Zocchi, E., Franco, L., and De Flora, A. (2001). Connexin 43 hemi channels mediate Ca^{2+}-regulated transmembrane NAD^{+} fluxes in intact cells. FASEB J. *15*, 10–12.

Buchanan, P.C., Boylan, K.L.M., Walcheck, B., Heinze, R., Geller, M.A., Argenta, P.A., and Skubitz, A.P.N. (2017). Ectodomain shedding of the cell adhesion molecule Nectin-4 in ovarian cancer is mediated by ADAM10 and ADAM17. J. Biol. Chem. *292*, 6339–6351.

Chou, M.F., and Schwartz, D. (2011). Biological sequence motif discovery using motif-x. Curr. Protoc. Bioinformatics *Chapter 13*, Unit 13.15–24.

Corda, D., and Di Girolamo, M. (2003). Functional aspects of protein mono-ADP-ribosylation. EMBO J. *22*, 1953–1958.

Davies, C.A., Perrett, D., Zhang, Z., Nielsen, B.R., Blake, D.R., and Winyard, P.G. (1999). Simultaneous analysis of nitrite, nitrate and the nicotinamide nucleotides by capillary electrophoresis: application to biochemical studies and human extracellular fluids. Electrophoresis *20*, 2111–2117.

Deshmukh, A.S., Murgia, M., Nagaraj, N., Treebak, J.T., Cox, J., and Mann, M. (2015). Deep proteomics of mouse skeletal muscle enables quantitation of protein isoforms, metabolic pathways, and transcription factors. Mol. Cell. Proteomics *14*, 841–853.

Eden, E., Navon, R., Steinfeld, I., Lipson, D., and Yakhini, Z. (2009). GOrilla: a tool for discovery and visualization of enriched GO terms in ranked gene lists. BMC Bioinformatics *10*, 48.

Fabrizio, G., Di Paola, S., Stilla, A., Giannotta, M., Ruggiero, C., Menzel, S., Koch-Nolte, F., Sallese, M., and Di Girolamo, M. (2015). ARTC1-mediated ADP-ribosylation of GRP78/BiP: a new player in endoplasmic-reticulum stress responses. Cell. Mol. Life Sci. *72*, 1209–1225.

Fasano, M., Curry, S., Terreno, E., Galliano, M., Fanali, G., Narciso, P., Notari, S., and Ascenzi, P. (2005). The extraordinary ligand binding properties of human serum albumin. IUBMB Life *57*, 787–796.

Feijs, K.L., Verheugd, P., and Lüscher, B. (2013). Expanding functions of intracellular resident mono-ADP-ribosylation in cell physiology. FEBS J. *280*, 3519–3529.

Glowacki, G., Braren, R., Cetkovic-Cvrlje, M., Leiter, E.H., Haag, F., and Koch-Nolte, F. (2001). Structure, chromosomal localization, and expression of the gene for mouse ecto-mono(ADP-ribosyl)transferase ART5. Gene *275*, 267–277.

Glowacki, G., Braren, R., Firner, K., Nissen, M., Kühl, M., Reche, P., Bazan, F., Cetkovic-Cvrlje, M., Leiter, E., Haag, F., and Koch-Nolte, F. (2002). The family of toxin-related ecto-ADP-ribosyltransferases in humans and the mouse. Protein Sci. *11*, 1657–1670.

Haag, F., Adriouch, S., Braß, A., Jung, C., Möller, S., Scheuplein, F., Bannas, P., Seman, M., and Koch-Nolte, F. (2007). Extracellular NAD and ATP: partners in immune cell modulation. Purinergic Signal. *3*, 71–81.

Hahl, P., Hunt, R., Bjes, E.S., Skaff, A., Keightley, A., and Smith, A. (2017). Identification of oxidative modifications of hemopexin and their predicted physiological relevance. J. Biol. Chem. *292*, 13658–13671.

Hottiger, M.O. (2015). Nuclear ADP-ribosylation and its role in chromatin plasticity, cell differentiation, and epigenetics. Annu. Rev. Biochem. *84*, 227–263.

Hottiger, M.O., Hassa, P.O., Lüscher, B., Schüler, H., and Koch-Nolte, F. (2010). Toward a unified nomenclature for mammalian ADP-ribosyltransferases. Trends Biochem. Sci. *35*, 208–219.

Hvidberg, V., Maniecki, M.B., Jacobsen, C., Højrup, P., Møller, H.J., and Moestrup, S.K. (2005). Identification of the receptor scavenging hemopexin-heme complexes. Blood *106*, 2572–2579.

Janes, P.W., Wimmer-Kleikamp, S.H., Frangakis, A.S., Treble, K., Griesshaber, B., Sabet, O., Grabenbauer, M., Ting, A.Y., Saftig, P., Bastiaens, P.I., and Lackmann, M. (2009). Cytoplasmic relaxation of active Eph controls ephrin shedding by ADAM10. PLoS Biol. *7*, e1000215.

Kawahara, R., Granato, D.C., Yokoo, S., Domingues, R.R., Trindade, D.M., and Paes Leme, A.F. (2017). Mass spectrometry-based proteomics revealed Glypican-1 as a novel ADAM17 substrate. J. Proteomics *151*, 53–65.

Koch, T., and Rüger, W. (1994). The ADP-ribosyltransferases (gpAlt) of bacteriophages T2, T4, and T6: sequencing of the genes and comparison of their products. Virology *203*, 294–298.

Koch-Nolte, F. (2015). Endogenous ADP-Ribosylation, First Edition (Springer International Publishing).

Koch-Nolte, F., and Ziegler, M. (2013). Physiology of ADP-ribosylation. FEBS J. *280*, 3483.

Koch-Nolte, F., Duffy, T., Nissen, M., Kahl, S., Killeen, N., Ablamunits, V., Haag, F., and Leiter, E.H. (1999). A new monoclonal antibody detects a developmentally regulated mouse ecto-ADP-ribosyltransferase on T cells: subset distribution, inbred strain variation, and modulation upon T cell activation. J. Immunol. *163*, 6014–6022.

Koch-Nolte, F., Glowacki, G., Bannas, P., Braasch, F., Dubberke, G., Ortolan, E., Funaro, A., Malavasi, F., and Haag, F. (2005). Use of genetic immunization

to raise antibodies recognizing toxin-related cell surface ADP-ribosyltransferases in native conformation. Cell. Immunol. *236*, 66–71.

Koch-Nolte, F., Adriouch, S., Bannas, P., Krebs, C., Scheuplein, F., Seman, M., and Haag, F. (2006). ADP-ribosylation of membrane proteins: unveiling the secrets of a crucial regulatory mechanism in mammalian cells. Ann. Med. *38*, 188–199.

Koch-Nolte, F., Kernstock, S., Mueller-Dieckmann, C., Weiss, M.S., and Haag, F. (2008). Mammalian ADP-ribosyltransferases and ADP-ribosylhydrolases. Front. Biosci. *13*, 6716–6729.

Koch-Nolte, F., Fischer, S., Haag, F., and Ziegler, M. (2011). Compartmentation of NAD+-dependent signalling. FEBS Lett. *585*, 1651–1656.

Laing, S., Unger, M., Koch-Nolte, F., and Haag, F. (2011). ADP-ribosylation of arginine. Amino Acids *41*, 257–269.

Larsen, S.C., Leutert, M., Bilan, V., Martello, R., Jungmichel, S., Young, C., Hottiger, M.O., and Nielsen, M.L. (2017). Proteome-wide identification of in vivo ADP-ribose acceptor sites by liquid chromatography-tandem mass spectrometry. Methods Mol. Biol. *1608*, 149–162.

Lau, E., Cao, Q., Ng, D.C., Bleakley, B.J., Dincer, T.U., Bot, B.M., Wang, D., Liem, D.A., Lam, M.P., Ge, J., and Ping, P. (2016). A large dataset of protein dynamics in the mammalian heart proteome. Sci. Data *3*, 160015.

Leidecker, O., Bonfiglio, J.J., Colby, T., Zhang, Q., Atanassov, I., Zaja, R., Palazzo, L., Stockum, A., Ahel, I., and Matic, I. (2016). Serine is a new target residue for endogenous ADP-ribosylation on histones. Nat. Chem. Biol. *12*, 998–1000.

Martello, R., Leutert, M., Jungmichel, S., Bilan, V., Larsen, S.C., Young, C., Hottiger, M.O., and Nielsen, M.L. (2016). Proteome-wide identification of the endogenous ADP-ribosylome of mammalian cells and tissue. Nat. Commun. *7*, 12917.

Menzel, S., Rissiek, B., Bannas, P., Jakoby, T., Miksiewicz, M., Schwarz, N., Nissen, M., Haag, F., Tholey, A., and Koch-Nolte, F. (2015). Nucleotide-induced membrane-proximal proteolysis controls the substrate specificity of T cell ecto-ADP-ribosyltransferase ARTC2.2. J. Immunol. *195*, 2057–2066.

Mi, H., Huang, X., Muruganujan, A., Tang, H., Mills, C., Kang, D., and Thomas, P.D. (2017). PANTHER version 11: expanded annotation data from Gene Ontology and Reactome pathways, and data analysis tool enhancements. Nucleic Acids Res. *45* (*D1*), D183–D189.

Nanni, P., Panse, C., Gehrig, P., Mueller, S., Grossmann, J., and Schlapbach, R. (2013). PTM MarkerFinder, a software tool to detect and validate spectra from peptides carrying post-translational modifications. Proteomics *13*, 2251–2255.

Okazaki, I.J., and Moss, J. (1999). Characterization of glycosylphosphatidylinositiol-anchored, secreted, and intracellular vertebrate mono-ADP-ribosyltransferases. Annu. Rev. Nutr. *19*, 485–509.

Osago, H., Yamada, K., Shibata, T., Yoshino, K., Hara, N., and Tsuchiya, M. (2009). Precursor ion scanning and sequencing of arginine-ADP-ribosylated peptide by mass spectrometry. Anal. Biochem. *393*, 248–254.

Panse, C., and Grossmann, J. (2012). protViz: Visualizing and Analyzing Mass Spectrometry Related Data in Proteomics, R package (Functional Genomics Center Zurich).

Paoli, M., Anderson, B.F., Baker, H.M., Morgan, W.T., Smith, A., and Baker, E.N. (1999). Crystal structure of hemopexin reveals a novel high-affinity heme site formed between two beta-propeller domains. Nat. Struct. Biol. *6*, 926–931.

Paone, G., Wada, A., Stevens, L.A., Matin, A., Hirayama, T., Levine, R.L., and Moss, J. (2002). ADP ribosylation of human neutrophil peptide-1 regulates its biological properties. Proc. Natl. Acad. Sci. USA *99*, 8231–8235.

Poulsen, J.W., Madsen, C.T., Young, C., Poulsen, F.M., and Nielsen, M.L. (2013). Using guanidine-hydrochloride for fast and efficient protein digestion and single-step affinity-purification mass spectrometry. J. Proteome Res. *12*, 1020–1030.

Rosenthal, F., and Hottiger, M.O. (2014). Identification of ADP-ribosylated peptides and ADP-ribose acceptor sites. Front. Biosci. *19*, 1041–1056.

Sakry, D., Neitz, A., Singh, J., Frischknecht, R., Marongiu, D., Binamé, F., Perera, S.S., Endres, K., Lutz, B., Radyushkin, K., et al. (2014). Oligodendrocyte precursor cells modulate the neuronal network by activity-dependent ectodomain cleavage of glial NG2. PLoS Biol. *12*, e1001993.

Scheuplein, F., Schwarz, N., Adriouch, S., Krebs, C., Bannas, P., Rissiek, B., Seman, M., Haag, F., and Koch-Nolte, F. (2009). NAD^+ and ATP released from injured cells induce P2X7-dependent shedding of CD62L and externalization of phosphatidylserine by murine T cells. J. Immunol. *182*, 2898–2908.

Seman, M., Adriouch, S., Haag, F., and Koch-Nolte, F. (2004). Ecto-ADP-ribosyltransferases (ARTs): emerging actors in cell communication and signaling. Curr. Med. Chem. *11*, 857–872.

Stevens, L.A., Levine, R.L., Gochuico, B.R., and Moss, J. (2009). ADP-ribosylation of human defensin HNP-1 results in the replacement of the modified arginine with the noncoded amino acid ornithine. Proc. Natl. Acad. Sci. USA *106*, 19796–19800.

Szklarczyk, D., Franceschini, A., Wyder, S., Forslund, K., Heller, D., Huerta-Cepas, J., Simonovic, M., Roth, A., Santos, A., Tsafou, K.P., et al. (2015). STRING v10: protein-protein interaction networks, integrated over the tree of life. Nucleic Acids Res. *43*, D447–D452.

Tolosano, E., and Altruda, F. (2002). Hemopexin: structure, function, and regulation. DNA Cell Biol. *21*, 297–306.

Ueda, K., and Hayaishi, O. (1985). ADP-ribosylation. Annu. Rev. Biochem. *54*, 73–100.

Vizcaíno, J.A., Csordas, A., del-Toro, N., Dianes, J.A., Griss, J., Lavidas, I., Mayer, G., Perez-Riverol, Y., Reisinger, F., Ternent, T., et al. (2016). 2016 update of the PRIDE database and its related tools. Nucleic Acids Res. *44* (*D1*), D447–D456.

Wiśniewski, J.R., Zougman, A., Nagaraj, N., and Mann, M. (2009). Universal sample preparation method for proteome analysis. Nat. Methods *6*, 359–362.

Yang, Z., Philips, J.D., Doty, R.T., Giraudi, P., Ostrow, J.D., Tiribelli, C., Smith, A., and Abkowitz, J.L. (2010). Kinetics and specificity of feline leukemia virus subgroup C receptor (FLVCR) export function and its dependence on hemopexin. J. Biol. Chem. *285*, 28874–28882.

Zolkiewska, A., and Moss, J. (1993). Integrin alpha 7 as substrate for a glycosylphosphatidylinositol-anchored ADP-ribosyltransferase on the surface of skeletal muscle cells. J. Biol. Chem. *268*, 25273–25276.

Zolkiewska, A., and Moss, J. (1995). Processing of ADP-ribosylated integrin alpha 7 in skeletal muscle myotubes. J. Biol. Chem. *270*, 9227–9233.

STAR★METHODS

KEY RESOURCES TABLE

REAGENT or RESOURCE	SOURCE	IDENTIFIER
Antibodies		
anti-FLAG antibody M2, mouse	Sigma	Cat# F1804; RRID: AB_262044
anti-ARTC1 antibody	Koch-Nolte et al., 2005	N/A
Chemicals, Peptides, and Recombinant Proteins		
Hemopexin protein, mouse, recombinant	Sino biological	Cat# 50271-M08H
ARTC1 protein, mouse, recombinant	Koch-Nolte et al., 2005	N/A
AF1521 protein, recombinant	Martello et al., 2016	N/A
PARG protein, recombinant	Martello et al., 2016	N/A
[32P] NAD+	Perkin Elmer	Cat# BLU023X250UC
Critical Commercial Assays		
RNAiMAX	Thermo Fisher Scientific	Cat# 13778030
NucleoSpin RNA II kit	Marchery-Nagel	Cat# 740955
High Capacity cDNA Reverse Transcription Kit	Applied Biosystems	Cat# 4368814
KAPA SYBR fast	Kapa Biosystems	Cat# 07959435001
Microcon-30-kDa-cutoff filter units	Millipore	Cat# MRCF0R030
Deposited Data		
Raw and analyzed mass spectrometry data	This study	ProteomeXchange: PXD008041
Experimental Models: Cell Lines		
C2C12 myoblasts, mouse	ATCC	Cat# CRL-1772
Mouse skeletal muscle and heart proteomics data	This study	ProteomeXchange: PXD008041
DC27.10 lymphoma cells overexpressing FLAG-tagged mouse ARTC1 or mouse ARTC3	Koch-Nolte et al., 2005	N/A
Experimental Models: Organisms/Strains		
C57BL/6 *ARTC1*−/−	This study	N/A
Software and Algorithms		
Proteome Discoverer, v2.1	Thermo Fisher Scientific	Cat# OPTON-30812
Mascot 2.5.1.3	matrixscience	http://www.matrixscience.com
Progenesis QI v. 3.0.6039.34628	Nonlinear dynamics	http://www.nonlinear.com
Scaffold v.4.7.2	Proteome software	http://www.proteomesoftware.com
Perseus software suite	Max Planck Institute of Biochemistry, Department of Proteomics and Signal Transduction, Munich	http://www.biochem.mpg.de/5111810/perseus
GOrilla	Eden et al., 2009	http://cbl-gorilla.cs.technion.ac.il
STRING v. 10.5	Szklarczyk et al., 2015	https://string-db.org/cgi/input.pl
PANTHER	Mi et al., 2017	http://pantherdb.org
PTM marker finder	Nanni et al., 2013	N/A
motif-x	Chou and Schwartz, 2011	http://motif-x.med.harvard.edu
Perseus software suite	Max Planck Institute of Biochemistry, Department of Proteomics and Signal Transduction, Munich	http://www.biochem.mpg.de/5111810/perseus
Other		
Orbitrap Fusion Tribrid mass spectrometer	Thermo Fisher Scientific	Cat# IQLAAEGAAPFADBMBCX
Orbitrap Q Exactive HF mass spectrometer	Thermo Fisher Scientific	Cat# IQLAAEGAAPFALGMBFZ
nano EasyLC 1000	Thermo Fisher Scientific	Cat# LC120

CONTACT FOR REAGENT AND RESOURCE SHARING

Further information and requests should be directed to and will be fulfilled by the Lead Contact, Michael O. Hottiger (michael.hottiger@dmmd.uzh.ch). For some items such as ARTC1-deficient mice MTAs may apply.

EXPERIMENTAL MODEL AND SUBJECT DETAILS

Generation and Characterization of Artc1$^{-/-}$ Mice

All chemicals were purchased from Sigma unless otherwise stated. Mice were obtained from the Animal Resources Units of the University of California at San Francisco and the University Medical Center, Hamburg. Experiments were performed in accordance with international guidelines on the ethical use of animals and were approved by the lcoal animal welfare commission (Amt für Verbraucherschutz, Lebensmittelsicherheit und Veterinärwesen Hamburg, Nr. 12/130). A targeting vector for the *Artc1* locus was constructed in which loxP sites were introduced up- and downstream of the *Artc1*-encoding exons 3 and 4 and a pgk-neomycin resistance cassette. The targeting construct was linearized with NotI and transfected into RF8 ES cells. Neomycin resistant clones were screened by Southern Blot analyses using informative 5′ and 3′ flanking probes. Two of 600 tested clones showed additional bands indicating homologous recombination at the target locus. Following injection of these ES cells into B6 blastocysts, chimeric male and female mice were obtained. Germline transmission of the targeted locus was obtained for both clones upon mating of chimeric and B6 mice. PCR analyses using primers flanking the distal loxP site confirmed the presence and Mendelian inheritance of this site. *Artc1* floxed mice were mated with mice expressing the cre recombinase under control of the β-actin promoter (deleter mice). PCR analyses using primers from the neomycin gene and the 3′ flanking region of the *Artc1* gene yielded a diagnostic band in progeny but not parental mice, indicating deletion of exons 3 and 4 in the targeted *Artc1* allele. *Artc1*$^{-/-}$ mice were backcrossed onto the C57BL/6 background for 12 generations.

Performance Assessment

Sex and age matched adult WT and *Artc1*$^{-/-}$ mice were monitored for voluntary activity using the Mouse E-Motion universal mobile datalogger system (INFRA-E-MOTION GmbH, Hamburg, Germany). Mice were placed in individual cages and movements were recorded in three consecutive 12 h light/12 h dark cycles. Endurance of muscle activity was assessed using the rotarod performance system (TSE systems, Bad Homburg, Germany). For this, mice were adapted to the rotarod at low speed (4 rpm) in trials 1 and 2. Trials 3-5 were then performed at an accelerated speed (8 rpm) with a pause of 45 min between each trial. Trial 6 was performed the next day at the accelerated speed. The maximum duration of mice on the rotarod was 5 min. Experiments were performed in accordance with international guidelines on the ethical use of animals and were approved by the local animal welfare commission (Amt für Verbraucherschutz, Lebensmittelsicherheit und Veterinärwesen Hamburg, Nr. 12/130).

Mouse Treatment and Organ Harvesting for Proteomic Experiment

WT and *ARTC1*$^{-/-}$ C57BL/6 mice were maintained on a 12-h light-dark cycle with regular unrestricted diet. WT (male, 15weeks) and *ARTC1*$^{-/-}$ (male, 9 weeks) mice were injected with 10 mg NAD^+ or stayed untreated and sacrificed after 30 min. Mice (n = 3 per group) were anesthetized with isoflurane and perfused with PBS containing 1 mM Novobiocin. Heart and skeletal muscle from legs were collected and immediately snap-frozen in liquid nitrogen. All samples were stored at −80°C. In order to optimize the analysis and to rule out ADP-ribosylation artifacts induced by stress and lysis, we evaluated different sample preparation methods and decided for a strongly denaturing Gnd-HCl lysis protocol and *in vivo* perfusion with the ARTC inhibitor Novobiocin. An additional Novobiocin treatment 30 min before euthanasia of the animals did not lead to further reduction in the ARTC1-dependent ADP-ribosylome and was thus judged to be unnecessary (Figure S4E). For untreated organ donors, untreated WT and *ARTC1*$^{-/-}$ C57BL/6 were maintained on a 12-h light-dark cycle with regular unrestricted diet. Organs of untreated animals were taken under license ZH207/2015 according to institutional and cantonal regulations.

Cell Culture and Treatments

The mouse skeletal muscle cell line C2C12 was maintained below 60% confluence in Dulbecco's modified Eagle's medium (DMEM) supplemented with 20% fetal calf serum and 1x penicillin/streptomycin (Invitrogen). For differentiation into myotubes, cells were grown until complete confluence and, subsequently, growth medium was exchanged for DMEM supplemented with 0.5% fetal calf serum and 1x penicillin/streptomycin (Invitrogen). This differentiation medium was exchanged every 24h until day 4 of differentiation. For transient knockdown of ARTC1 or ARTC3, about 1 million C2C12 cells were seeded per 6 cm dish and transfected with siRNA against either ARTC1, ARTC3 or a scrambled siRNA using lipofectamine RNAiMAX (Invitrogen) according to the manufacturer's manual. For the NAD^+ treatment, differentiated myotubes were washed twice with serum free DMEM and subsequently treatment was performed for 30 min in serum free DMEM containing either 1 or 50 μM NAD^+.

Wild-type DC27.10 lymphoma cells (Koch-Nolte et al., 2005), as well as DC27.10 cells overexpressing either FLAG-tagged mARTC1 or mARTC3 were cultured in RPMI medium supplemented with 10% FCS and 1x penicillin/streptomycin (Invitrogen).

Primary myoblasts were isolated from hindlimbs and forelimbs of neonatal mice (2-5 days old). The muscle tissue was incubated in Dulbecco's phosphate-buffered saline (DPBS) with 1% collagenase II (Invitrogen), 2.4U/ml dispase II (Roche) and 2.5 mM $CaCl_2$ for

45 min at 37°C, and then passed through 100 μm-nylon mesh filter (BD Biosciences). The filtrate was centrifuged, the cell pellet was suspended in Ham's F-10 medium (Cambrex) containing 20% FBS and 1% penicillin/streptomycin, pre-plated for 30 min on collagen I-coated plates, and then plated on tissue culture-treated plastic plates. To stimulate differentiation of myoblasts to myotubes, 90%–100% confluent myoblasts were incubated for 3 days in medium containing 2% horse serum.

METHOD DETAILS

Gene Expression

RNA extraction was performed with the NucleoSpin RNA II kit (Macherey-Nagel). Mouse tissue samples were lysed using a tissue lyser II (QIAGEN) with the provided lysis buffer. C2C12 myotubes were washed with PBS, before lysis with the same buffer. After RNA extraction RNA was quantified with a NanoDrop (Thermo Fisher Scientific) and reverse transcribed according to the supplier's protocol (High Capacity cDNA Reverse Transcription Kit, Applied Biosystems). Quantitative real-time polymerase chain reactions (qPCR) were performed with KAPA SYBR fast (Kapa Biosystems) and a Rotor-Gene Q 2plex HRM System (QIAGEN).

Flow Cytometry

Two million DC27.10 cells per condition (WT, ARTC1/3) were stained with an anti-FLAG antibody (M2, Sigma) diluted 1:750 in PBS containing 2% BSA for 30 min on ice. Cells were further washed 3 times and stained with a secondary antibody conjugated to A488 (Biolegend) for another 30 min on ice in the dark. After 3 washes, cells were resuspended in 500 μl PBS and analyzed via flow cytometry using a FACSCanto (BD Biosciences).

Immunoblotting

Three-month old wild-type and *Artc1*$^{-/-}$ mice were euthanized by CO_2 inhalation in accordance with a protocol approved by the Kansas State University Institutional Animal Care and Use Committee. Hind limb muscles were excised, ground, and homogenized in 50 mM Tris-Cl, pH 7.4, 150 mM NaCl, 50 mM octylglucoside, 1 mM AEBSF, 5 μg/ml aprotinin, 5 μg/ml leupeptin, 5 μg/ml pepstatin A (5 mL homogenization buffer/1 g tissue). The homogenate was centrifuged at 13,000 g for 20 min, the supernatant was filtered through a 0.45 μm filter, and incubated with 0.2 mL of Concanavalin A agarose beads at 4°C for 2 h with gentle shaking. The beads were washed with 5 mL of homogenization buffer and eluted with SDS-PAGE loading buffer, the eluate was resolved by SDS-PAGE and transferred to a nitrocellulose membrane. The membrane was blocked with 3% (w/v) dry milk and 0.3% (v/v) Tween-20 in DPBS, then incubated with anti-ARTC1 antibody (Koch-Nolte et al., 2005) in blocking buffer, followed by incubation with horseradish peroxidase-labeled secondary antibody and detection using the WestPico chemiluminescence kit (Pierce).

ADP-Ribosylation Reaction on Cells

Differentiated primary myoblasts (myotubes) were washed with DPBS and incubated for 30 min in DPBS (with Ca^{2+} and Mg^{2+}) containing 5 μM [adenylate-^{32}P] NAD^+ and 1 mM ADP-ribose. Cellular proteins were extracted with extraction buffer (50mM Tris-HCl, pH 7.4, 150 mM NaCl, 1 mM ADP-ribose, 1% Triton X-100, 1% sodium deoxycholate, 0.1% SDS, 1 mM 4-(2-aminoethyl)-benzene-sulfonylfluoride hydrochloride (AEBSF), 5 μg/ml aprotinin, 5 μg/ml leupeptin, 5 μg/ml pepstatin A, 10 mM 1,10-phenanthroline; 0.5 mL extraction buffer/well in a 6-well plate). Cell extracts were centrifuged at 21,000 g for 15 min, and supernatants were analyzed by autoradiography after SDS-PAGE under reducing conditions.

C2C12 myotubes pretreated with siRNA against either ARTC1, ARTC3 or a control siRNA were washed twice with serum free DMEM and subsequently incubated for 30 min with [^{32}P]-NAD^+ (2 μCi and 1 μM NAD^+/dish) at 37°C. After treatment, cells were washed 3 times with serum free DMEM and membrane proteins were isolated by incubating the cells for 20 min on ice in presence of 200 μl membrane solubilization buffer (PBS, 1% Triton X-100, Roche Protease Inhibitor, 100 μM Novobiocin and 10 μM PJ34). Lysed cells were further detached from the plates by scraping and centrifuged for 15 min at 13,000 g to remove insoluble material. The supernatants were analyzed via autoradiography after SDS-PAGE under denaturing conditions.

Six million DC27.10 cells per condition (WT, ARTC1/3 overexpressing) were incubated in the presence of [^{32}P]-NAD^+ and processed as described for the C2C12 cells with the exception that, being suspension cells, DC27.10 cells had to be centrifuged down for each washing step.

ADP-Ribosylation Reaction with Recombinant Proteins

Recombinant mouse ARTC1 was purified from DC27.10 lymphoma cells stably transfected with FLAG-tagged ARTC1 (Koch-Nolte et al., 2005). DC27.10_ARTC1 cells were incubated with Phospholipase C (Sigma) for 1 h at 37°C. Cell supernatants were clarified by centrifugation (20 min, 13000 g) and ARTC1 was purified by affinity chromatography on agarose immobilized anti-FLAG mAb M2 (Sigma). The column was washed with PBS, 1% Triton X-100 and ARTC1 was eluted with 100 mM glycine, 10 mM Tris (pH 2.7). The eluate was neutralized with one-tenth volume of 1 M Tris (pH 9.0) and the buffer was exchanged to PBS by gel filtration (PD-10 columns; Pharmacia). ARTC1 was concentrated using centrifugal filters (Millipore; molecular weight cutoff 10 kDa). Recombinant mouse hemopexin was purchased from Sino Biological. To monitor trans ADP-ribosylation of HPX by radiography we incubated 50 nM ARTC1 with 2.5 μM HPX using 0.5 μCi [^{32}P]-NAD^+ (Perkin Elmer) in PBS and incubated at 37°C for 30 min or 60 min. For some reactions 10 μM Novobiocin or 10 μM heme was added. Reactions were stopped by adding SDS-loading buffer,

with subsequent boiling at 95°C for 5 min. Samples were run on an SDS-PAGE gel, stained with Coomassie blue, photographed, destained, and exposed on phosphorscreens overnight. Images were taken with a Typhoon FLA 9400 phosphorimager (GE Healthcare).

For the Heme-HPX binding assay as well as for subsequent MS analysis 10 μM HPX was incubated with 100 μM NAD^+ with or without 250 nM ARTC1 in PBS, overnight at 37°C. The next day, indicated amounts of heme were added to the reaction, incubated at 37°C and absorbance was measured with a NanoDrop (Thermo Fisher Scientific) and the OD at 413 nM was quantified for the different reactions. All reactions were done and measured as independent triplicates.

ADPr-Peptide Enrichment

C2C12 cells were washed twice with PBS and subsequently lysed and scraped by adding 95°C Gnd-HCL-lysis buffer (6 M guanidine-hydrochloride, 5 mM tris(2-carboxyethyl)phosphine (TCEP), 10 mM chloroacetamide (CAA), in 100 mM Tris pH 8). Frozen murine heart and skeletal muscle samples were added to 95°C Gnd-HCL-lysis buffer and ground in a tissue lyser II (QIAGEN), for 3 min at 30hz. Samples were subsequently incubated at 95°C for 10 min and sonicated for 1 min at an amplitude of 30%. Lysate was cleared by centrifugation at 4000 g, ten times diluted with 25 mM Tris pH 8, and digested with sequencing grade trypsin (Promega). The peptide mixture was treated with PARG enzyme to reduce potentially PARylated peptide to MARylated peptides, and the peptides were enriched using an Af1521 macrodomain affinity enrichment and prepared for MS analysis as described previously (Martello et al., 2016). The *in vitro* modified HPX protein was processed using filter aided sample preparation (FASP) protocol using Microcon-30-kDa-cutoff filter units (Millipore) and sequencing grade trypsin (Promega) (Wiśniewski et al., 2009).

Liquid Chromatography and Mass Spectrometry Analysis

Identification of ADP-ribosylated peptides from C2C12, skeletal muscle, heart and recombinant HPX was performed on an Orbitrap Fusion Tribrid mass spectrometer (Thermo Fisher Scientific), coupled to a nano EasyLC 1000 liquid chromatograph (Thermo Fisher Scientific). We applied an ADP-ribose product-dependent method called HCD-PP-EThcD (Bilan et al., 2017a) Briefly, the method includes high-energy data-dependent HCD, followed by high-quality HCD and EThcD MS/MS when two or more ADP-ribose fragment peaks (136.0623, 250.0940, 348.07091, and 428.0372) were observed in the HCD scan. A detailed description of the MS parameters can be found in (Bilan et al., 2017a). Solvent compositions in channels A and B were 0.1% formic acid in H2O and 0.1% formic acid in acetonitrile, respectively. Peptides were loaded onto an Acclaim PepMap 100 (Thermo Scientific) trap column, 75 μm x 2 cm, packed with C18 material, 3 μm, 100 Å, and separated on an analytical EASY-Spray column (Thermo Scientific, 75 μm × 500 mm) packed with reverse-phase C18 material (PepMap RSLC, 2 μm, 100 Å). Peptides were eluted over 110 min at a flow rate of 300 nL/min. An elution gradient protocol from 2% to 25% B, followed by two steps at 35% B for 5 min and at 95% B for 5 min, respectively, was used.

Heart samples were additionally analyzed using an Orbitrap Q Exactive HF mass spectrometer (Thermo Fisher Scientific) coupled to a nano EasyLC 1000 (Thermo Fisher Scientific). The peptides were loaded onto a reverse-phase C18 (ReproSil-Pur 120 C18-AQ, 1.9 μm, Dr. Maisch GmbH) packed self-made column (75 μm × 150 mm) that was connected to an empty Picotip emitter (New Objective, Woburn, MA). Peptides were injected into the MS at a flow rate of 300 nL/min and were separated using a 90 min gradient of 2% to 25% buffer B. The MS was set to acquire full-scan MS spectra (300–1700 *m/z*) at a resolution of 60,000 after accumulation to an automated gain control (AGC) target value of 3×10^6. Charge state screening was enabled, and unassigned charge states and single charged precursors were excluded. Ions were isolated using a quadrupole mass filter with a 2 m/z isolation window. The maximum injection time was set to 240 ms and HCD fragmentation was performed at 28% normalized collision energy. Finally, selected ions were dynamically excluded for 20 s.

QUANTIFICATION AND STATISTICAL ANALYSIS

Raw Mass Spectrometry Data Analysis and Label Free Quantification

MS and MS/MS spectra were converted to Mascot generic format (MGF) by use of Proteome Discoverer, v2.1 (Thermo Fisher Scientific, Bremen, Germany). When multiple fragmentation techniques (HCD and EThcD) were utilized, separate MGF files were created from the raw file for each type of fragmentation. MGF files were further processed (Bilan et al., 2017a). The MGFs were searched against the UniProtKB mouse database (taxonomy 10090, version 20160902), which included 24'905 Swiss-Prot, 34'616 TrEMBL entries, 59'783 reverse sequences, and 262 common contaminants.

Mascot 2.5.1.3 (Matrix Science) was used for peptide sequence identification with previously described search settings and some modification for the EThcD searches (Bilan et al., 2017a). Enzyme specificity was set to trypsin, allowing up to 4 missed cleavages. The ADP-ribose variable modification was set to a mass shift of 541.0611, with scoring of the neutral losses equal to 347.0631 and 249.0862. The marker ions at m/z 428.0372, 348.0709, 250.0940, 136.0623 were ignored for scoring. Ser, Arg, Lys, Asp and Glu residues were set as variable ADP-ribose acceptor sites. Carbamidomethylation was set as a fixed modification on C and oxidation as a variable modification on M. Peptides are considered correctly identified when a Mascot score > 20 and an expectation value < 0.05 are obtained. For the ADP-ribosylation site analyses, peptides identified with EThcD fragmentation, having a mascot localization score > 90% were used if not stated otherwise.

To perform label-free quantification based on the MS1 precursor peak area of the identified peptides and proteins, Progenesis QI software (v. 3.0.6039.34628, Nonlinear Dynamics, Purham, NC) was applied. Raw data were imported into Progenesis and aligned based on the MS1 peak retention time. All samples were normalized based on the total signal intensity. The obtained results were exported as MGF and searched with Mascot as indicated above. The Mascot search results were imported into Scaffold software (v.4.7.2) and filtered for protein and peptide FDR values of 1% and 0.5% respectively. When multiple precursors were observed for the same peptide, the values were summed up to obtain the total level of the peptide.

Bioinformatic Analyses

Statistical analysis, volcano plot analysis, principal component analysis and hierarchical clustering were performed using the Perseus software suite (Max Planck Institute of Biochemistry, Department of Proteomics and Signal Transduction, Munich). Normalized LFQ intensities were imported.

For GO enrichment analyses the GOrilla online tool (Eden et al., 2009) was applied, using a C2C12 myotube, a mouse skeletal muscle or a mouse heart proteome as background (Deshmukh et al., 2015; Lau et al., 2016). A p value threshold of 10^{-3} was set and higher-ranking terms were chosen from GO Biological Processes, GO Molecular Functions, GO Cellular Compartments or Kyoto Encyclopedia of Genes and Genomes (KEGG) for display.

Protein-protein interactions in between ADP-ribosylated protein were analyzed using the interaction data from the STRING database (v. 10.5) using high confidence interaction scores (≥ 0.7) and hiding disconnected ADP-ribosylated nodes from the network. Significantly enriched, interesting GO Biological Processes and KEGG pathway terms were annotated according to the STRING database and GO Cellular Compartments were annotated using the PANTHER database (Mi et al., 2017).

The heart samples measured on the Q Exactive HF MS, using a non-product dependent HCD fragmentation method, were used to extract MS2 ADP-ribose marker ion patterns from the Mascot ouput.dat files. For this we used the PTM marker finder tool and following marker ions were included 136.0618, 250.0935, 348.0704, 428.0367 and 584.0901 (Nanni et al., 2013). Only spectra were considered where at least four marker ions were identified with an intensity of at least 5% of the highest peak and a mascot score of > 20.

For the ADP-ribosylation site motif analysis we used the web-based motif-x program (Chou and Schwartz, 2011). We included all Arg-ADPr sites identified with a localization score > 90% for the analysis. A p value threshold < 0.0005 was chosen for the binomial probability and a 21 amino acid window with the ADP-ribosylation site in the center was analyzed against the whole mouse proteome as a background. All identified motifs were reported as a 13 amino acid window. Their fraction to all analyzed sites is indicated as well as the motif score. The motif score is the sum of the negative log probabilities used to fix each position of the reported motif. The higher the score the more statistically significant and specific is the motif.

The protein structure of HPX (Paoli et al., 1999) was visualized and annotated using PyMOL v1.7.4. All Venn diagrams were generated using biovenn (http://www.biovenn.nl).

DATA AND SOFTWARE AVAILABILITY

Data Availability

The accession number for the mass spectrometry proteomics data for the C2C12 cells, the mouse skeletal and heart muscle tissues, including the RAW files, peak list files (MGFs), and result files (mzIdent) reported in this paper is ProteomeXchange PRIDE: PXD008041 (10.6019/PXD008041) (Vizcaíno et al., 2016). The additional data that support the findings of this study are available from the corresponding author on request.